

POLITECNICO DI TORINO

Department of Electronics and Telecommunications

Telecommunications Engineering

Master Thesis

**Single mode-Multimode-Single mode
optical Fiber sensors**



Supervisors:

Dr. Massimo Olivero

prof. Guido Perrone

Candidate:

Makan Mohammadi Ostadkalayeh

201977

Oct 2020

Acknowledgements

I would like to convey my sincere appreciation and heartfelt gratitude to Massimo Olivero for his priceless advice and encouragements also Prof. Perrone for his help and supervision. Last but not least, deep and sincere gratitude to Sahar Mouzari for her continuous and unparalleled love, helps and supports.

”Shortly after I finished this book, my dear son Marc, five years old, was taken from me. I dedicate *All That Is Solid Melts into Air* to him. His life and death bring so many of its ideas and themes close to home: the idea that those who are most happily at home in the modern world, as he was, may be most vulnerable to the demons that haunt it; the idea that the daily routine of playgrounds and bicycles, of shopping and eating and cleaning up, of ordinary hugs and kisses, may be not only infinitely joyous and beautiful but also infinitely precarious and fragile; that it may take desperate and heroic struggles to sustain this life, and sometimes we lose. Ivan Karamazov says that, more than anything else, the death of children makes him want to give back his ticket to the universe. But he does not give it back. He keeps on fighting and loving; he keeps on keeping on.”

Marshall Berman, *All That is Solid Melts Into Air*

Abstract

In this thesis, we study the theory of waveform deformation in sensors and the effect of heat on them in a practical experience while constructing a variety of sensors which the multimode part includes BIF, Coreless fiber, SM2000 fiber, multimode fiber With 5 ° C thermal intervals, we study the effect of heat on the shape of the power spectrum. These changes include changes in wavelengths and shifts in power levels.

What matters in this review is: first of all which one of these sensors is most sensitive to heat, the sensitivity is measurable by comparing the wavelength shift and power. Second, which sensors have a more stable behavior when we increase the temperature uniformly, in other words, they show a more linear behavior. The third point is that in this research, it is noted whether the sensor will return to its original state when cooling back to the room temperature or not, and if the answer is negative, how much difference is observable in comparison with the wavelength and power in the Power Spectrum graph.

At the end of this research, we will explore some areas of futuristic research in this field. Our method in this study is based on practical and laboratory data that includes the SMS sensor components fabricating in the form of misaligned and aligned, sensor mounting on a heater, installation of heater and power meter spectrometers, measurement of the numerical data effects of heat on the wavelength and power and finally the numerical analysis of the data and compare them together.

Contents

| | | |
|----------|--|-----------|
| 1 | Fundamental theories introducing SMS sensors characteristic | 3 |
| 1.1 | Multimode Interference (MMI) effects | 3 |
| 1.2 | MMI in optical fiber | 5 |
| 1.3 | MPA of SMS structures | 6 |
| 1.4 | SMS structures for interrogation of FBG sensors | 9 |
| 1.5 | Sensing applications of SMS fiber structures | 12 |
| 1.6 | Effect of misalignment on an SMS | 13 |
| 1.7 | Misalignment limits for a singlemode-multimodesinglemode fiber-based edge filter | 14 |
| 1.8 | SMS-based edge filters | 16 |
| 1.9 | Modal propagation analysis | 19 |
| 1.10 | Design example and spectral response | 20 |
| 1.11 | Temperature effect on SMS sensors (BIF as sample) | 22 |
| 1.12 | SMF-BIF-SMF Sensor Setup | 25 |
| 1.13 | SMF-BIF-SMF Sensor Characterization | 26 |
| 2 | Analyzing experimental result of temperature effect on various SMS sensors fiber | 30 |
| 2.1 | Framework | 30 |
| 2.2 | Producing SMS Fiber Sensor | 31 |
| 2.3 | SMS BIF | 33 |
| 2.4 | SMS Coreless Fiber | 40 |
| 2.5 | Single-mode Multi-mode Single-mode Sensor Fiber | 45 |
| 2.6 | SM2000 | 52 |

| | |
|-----------------------|-----------|
| 3 Conclusion | 57 |
| 4 Future Study | 59 |
| Bibliography | 62 |

Chapter 1

Fundamental theories introducing SMS sensors characteristic

1.1 Multimode Interference (MMI) effects

MMI is a useful concept in the implementation of some optical waveguide devices. At first, MMI was investigated and proposed for planar waveguides to develop optical signal processing applications, and optical sensing applications. To comprehend more about MMI, self-imaging phenomena should be studied. Self-imaging is defined as a property of multimode waveguides where an input field profile is reproduced due to the constructive interference which form single or multiple images of the singlemode input field along the propagation guide direction at periodic intervals. Self-imaging in a planar waveguide was analyzed using three methods: modal propagation analysis (MPA) [32], hybrid method [5], and the beam propagation method (BPM) [44]. MPA is a comprehensive theoretical tool describing self-imaging phenomena in multimode waveguides [32]. It also provides an insight into the mechanism of multimode interference as well as the basis for the numerical modelling and design.

Fig 1.1 illustrate self-imaging due to MMI in fact a multimode waveguide placed between input and output singlemode waveguides. The waveguide parameters are also shown in Fig 1.1, W_M is the width of the multimode waveguide and W_s is the width of the singlemode waveguide. Finally L is the length of the multimode waveguide. Exploiting MPA according to [32] an input field profile existing

at $Z = 0$ is decomposed into the modal distribution of all possible modes in the multimode waveguide. At a distance $Z = L$, the field profile can be expressed as a superposition of the modal distribution of all possible modes. The field at $Z = L$ will be a reproduction or self-image of the input field at $Z = 0$ Under certain circumstances. Fig. 1.2 demonstrates the simulated field profile within the multimode section and clearly self-imaging of the input field took place therefore at periodic intervals, a single image of the input field is reproduced. This occurs in Fig. 1.2 at 2708, 5415, and 8122 μm . Multi-fold images of the input field can also be found, for example, two-fold images can be found at 1354, 4062, 6770 and 9478 μm . Self-imaging happens at specific lengths only for certain wavelengths. The spectral response of an MMI-based device is therefore not flat and in fact has a bandpass type response, where the bandpass wavelength peak corresponds to the value where self-imaging distance is exactly equal to the multimode section length [32].

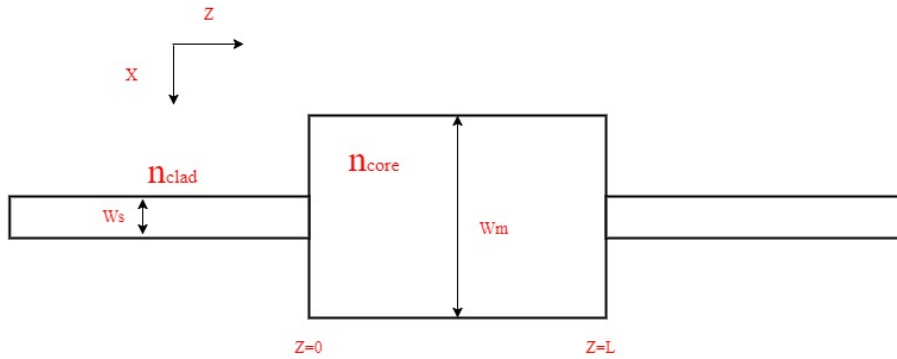


Figure 1.1

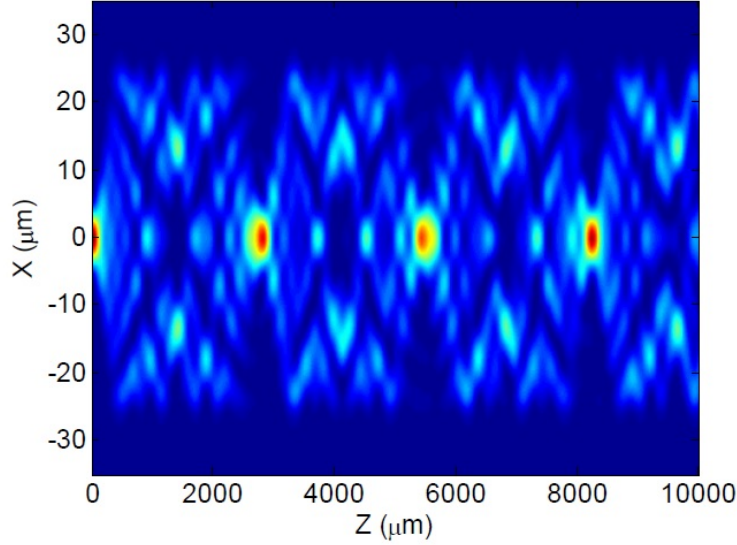


Figure 1.2

1.2 MMI in optical fiber

MMI can be implemented using a fiber hetero-structure such as singlemode-multimode-singlemode (SMS) fiber structure with a step index profile [38], [22]. An SMS fiber structure is fabricated by splicing a multimode fiber (MMF) between two singlemode fibers (SMFs). Fig. 1.3 shows a schematic of an SMS fiber structure. SMS fiber structures can either utilize a step index or a graded index profile MMF. SMS fiber structures utilizing a step index MMF section are considered in this text. The primary reason for this selection is that the spectral response of a step index MMF is more applicable for the development of edge filters [30].

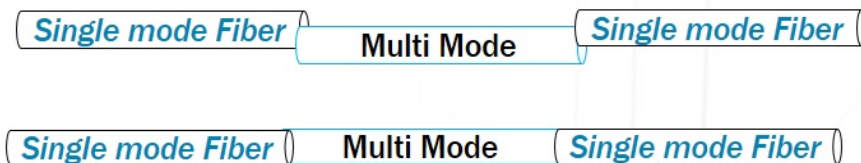


Figure 1.3

The MMF supports many guided modes and the input field to the MMF section is reproduced as single or multiple images along the propagation direction due to the interference between guided modes at periodic intervals. MMI in fiber

optics was analyzed using the MPA in cylindrical coordinates in [22].

1.3 MPA of SMS structures

To start with MPA exploiting cylindrical coordinates for the SMS fiber structure, the input beam to the MMF section is assumed to have a field distribution $\psi(r, 0)$ which is equal to the fundamental mode of the SMF. The input field can be decomposed into the eigenmodes of LP_{nm} of the MMF when the beam enters the MMF section. The eigenmodes and eigenvalues of the MMF can be calculated by the equations according to [22]. based on the input field circular symmetry and the assumption of perfect alignment of the central axes of the fibers cores of the SMF and MMF, only LP_{0m} can be excited. The reduction in the number of modes helps in reducing the computational complexity and time.

The field profile of LP_{0m} is defined as $F_v(r)$ and the eigenmodes of the MMF are normalized as $\int_0^\infty |\psi(r, 0)|^2 r dr = \int_0^\infty |F_v(r)|^2 r dr, v = 1, 2, \dots, m - 1$ where m is the number of modes in the MMF. The number of excited modes of LP_{0m} can be calculated using $m \approx \frac{V}{\pi}$ where $V = \frac{2\pi}{\lambda} a \sqrt{n_{core}^2 - n_{clad}^2}$ is the normalized frequency, λ is the wavelength in the free space, a is the core diameter, n_{core} and n_{clad} is the core and cladding refractive index of the MMF respectively. The input field at the MMF can be written as:

$$\psi(r, 0) = \sum_{v=0}^{m-1} c_v F_v(r) \quad (1.1)$$

where c_v is the excitation coefficient of each mode. The coefficient can be calculated by an overlap integral between $\psi(r, 0)$ and $F_v(r)$ so:

$$c_v = \frac{\int_0^\infty \psi(r, 0) F_v(r) r dr}{\int_0^\infty F_v(r, 0) F_v(r) r dr} \quad (1.2)$$

The field at a propagation distance z in the MMF section can be calculated:

$$\psi(r, z) = \sum_{v=0}^{m-1} c_v F_v(r) \exp(j\beta_v z) \quad (1.3)$$

Where β_v is the propagation constant of each MMF eigenmode. The propagation constant can be calculated from the MMF eigenvalues [3]. The transmission

loss in dB can be obtained using overlap integral method between $\psi(r, z)$ and the output SMF eigenmode $E_0(r)$ [39].

$$L_s(z) = 10 \cdot \log_{10} \left(\frac{|\int_0^\infty \psi(r, z) E_0(r) r dr|^2}{\int_0^\infty |\psi(r, z)|^2 r dr \int_0^\infty |E_0(r)|^2 r dr} \right) \quad (1.4)$$

Self-imaging happens at the so called self-imaging distance Lz . $zLL010$ is a beat length between the first two eigenmodes and L are the first two MMF propagation constants [22]. For instance, assume the SMF type is SMF28 with core diameter of 8.3 μm and MMF type is AFS105/125Y with core diameter of 105 μm . Fig. 1.4 and 1.5 display the light propagation in the MMF and corresponding transmission loss/coupling loss of the SMF output as a functions of MMF length, respectively. The self-imaging distance is 4.28 cm for a wavelength of 1550 nm shown in Fig. 1.4.

In self-imaging distance, the input field (at a propagation distance of 0 cm) is reproduced and hence, the transmission loss/coupling loss is approximately zero. For a fixed MMF length, SMS fiber structure produces a wavelength dependent spectral response. The spectral response of the SMS fiber structure is shown in Fig 1.6 for a wavelength range of 1500 to 1600 nm. It is obvious that the SMS fiber structure produces a bandpass spectral response and thus can be used as a bandpass filter [38],[22].

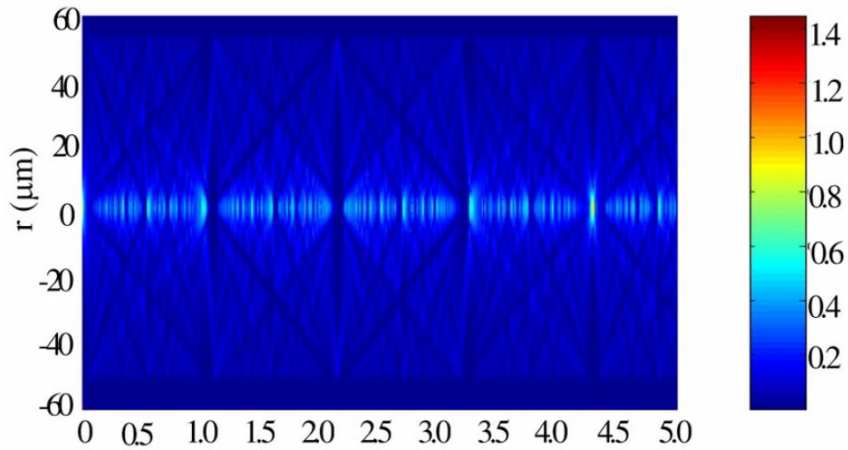


Figure 1.4

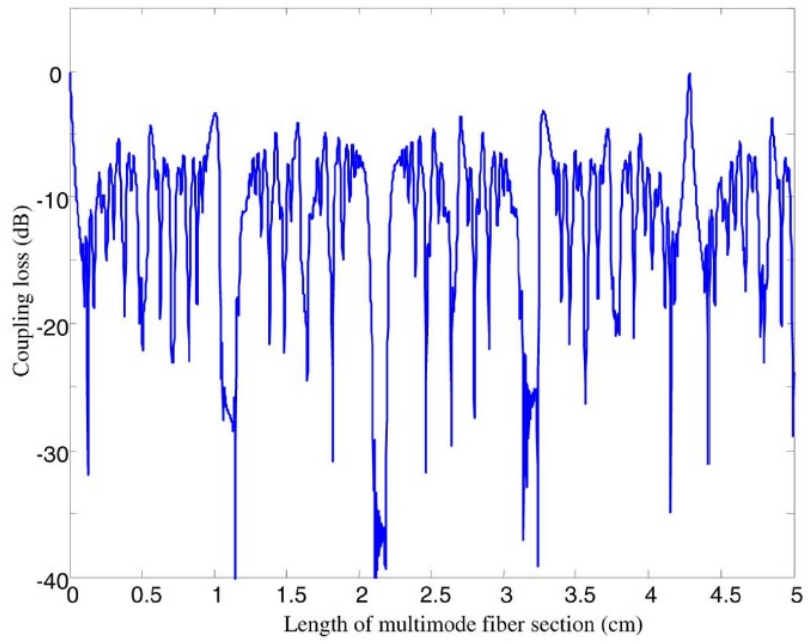
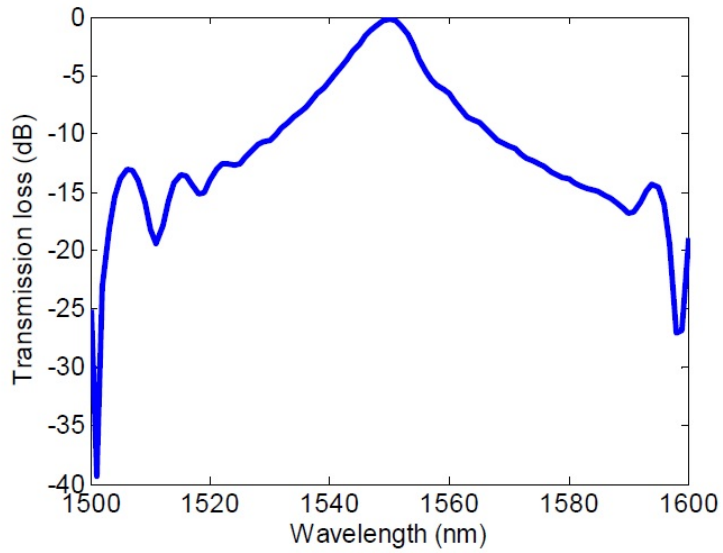


Figure 1.5



(c)

Figure 1.6

1.4 SMS structures for interrogation of FBG sensors

A wavelength measurement system is required for FBG sensor in order to extract temperature or strain information. Fig. 1.7 displays a typical configuration of an FBG-based sensor system. Light inserted from the broadband source via a circulator into the fiber containing the FBG. Only one wavelength is reflected back from the FBG and the reflected wavelength shift due to the changes in temperature or strain is monitored in a wavelength discriminator. A wavelength discriminator provides a known stable relationship between attenuation and wavelength, with this assumption and with a suitable calibration, the wavelength can be measured by means of an intensity measurement.

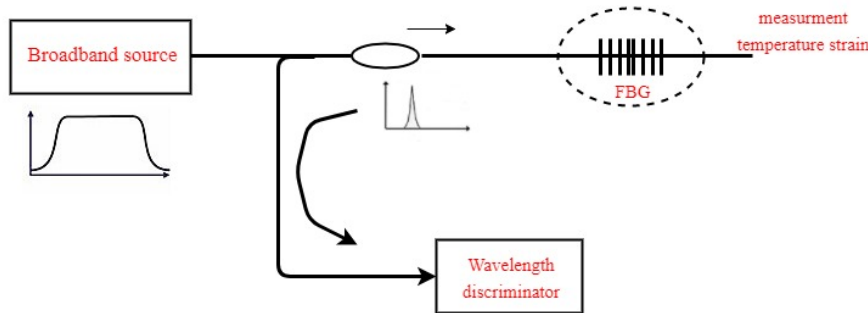


Figure 1.7

The general properties of an ideal discriminator in a wavelength measurement system are as follows: high resolution (more than 10 pm), high accuracy, high measurement speed to allow dynamic strain measurement and cost effectiveness. More over a wide wavelength range (more than 10 nm) is required where wavelength division multiplexed FBGs are used.

The ratio metric power measurement technique is an approach to wavelength discrimination that satisfies the mentioned requirements [28]. Evaluating wavelength-scanning-based active measurement scheme, its simple configuration, the potential for high-speed measurement, the absence of mechanical movement, and a low cost are its advantages [28]. Conventionally, A ratio metric wavelength monitor composed of a splitter which has two outputs, one attached to an edge filter arm with a well-defined spectral response and the other one attached to a reference

arm [28]. At the end of each arms a photo detector is placed. An unknown input signal wavelength can be measured by the electrical outputs ratio of the two photo detectors, assuming a suitable calibration.

Fig. 1.8 displays schematic structure of a typical ratio metric wavelength measurement system. A modified ratio metric wavelength measurement system including two edge filter arms with opposite slope spectral responses is also displays in Fig. 1.9. Exploiting the two edge filters can increase sensitivity and resolution of wavelength measurements [?]. Fig. 1.10 illustrates the spectral responses of the edge filters and the reference arm in a wavelength range from λ_L to λ_H . The corresponding ratio of the two outputs over the wavelength range are presented in Fig. 1.11 for the systems with one and two edge filters.

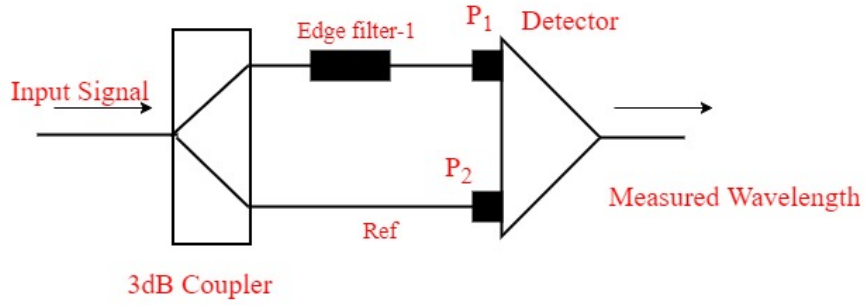


Figure 1.8

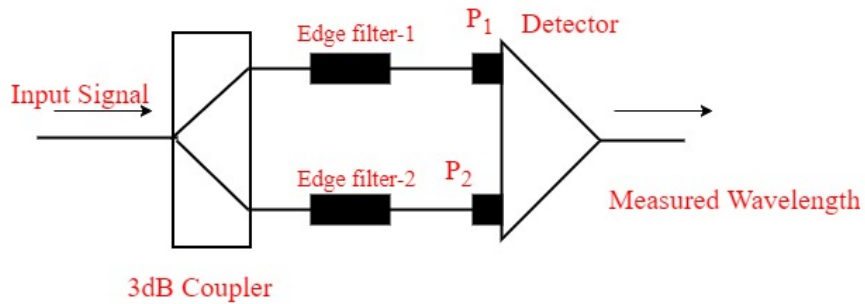


Figure 1.9

An SMS fiber structure is studied as a new type of an edge filter. Previous studies discussed that an SMS fiber can be operated as a bandpass filter[38],[22]. On either side of the centre wavelength in the bandpass response displayed in Fig. 1.6, the spectral responses monotonically increasing or decreasing over a specific wavelength range which can be utilized as a positive or negative slope edge filter.

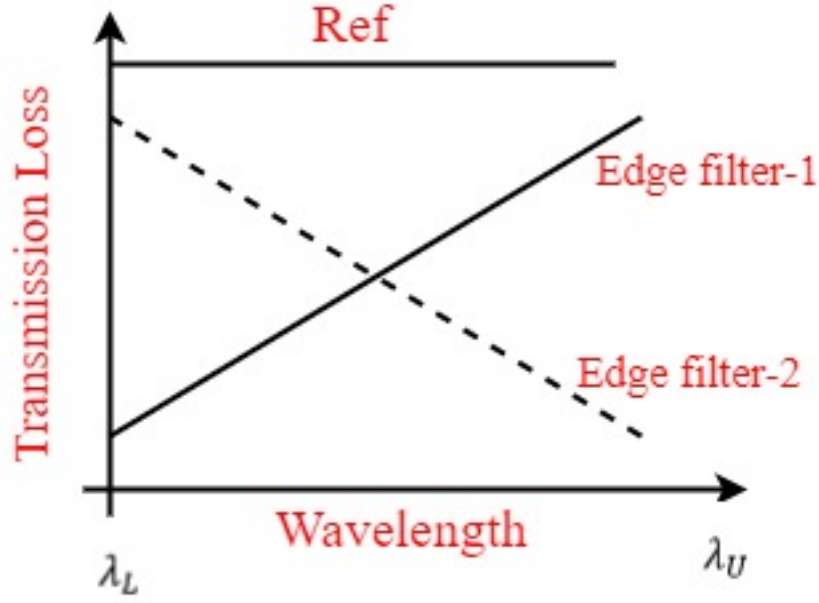


Figure 1.10

Several factors, such as noise, polarization dependent loss (PDL), and temperature dependent loss (TDL) can influence the resolution and accuracy of wavelength measurement in an all-fiber ratio metric system [20]-[8]. In [25], an acceptable slope for the edge filter is specified by the input signal-tonoise ratio (SNR). The photo detectors noise affects the resolution of the ratio metric wavelength measurement system as well [24]. In [24], demonstrated theoretically and experimentally that the source signal SNR, the photo detectors noise and the other sources noise such as receiver shot and thermal noise have a significant affect on the resolution of the wavelength measurement.

In an all-fiber ratio metric wavelength measurement system, polarization dependency can also degrade measurement accuracy [9]. In standard optical fibers, the state of polarization varies. For a macrobending fiber-based edge filter, the fiber structure needs to be optimized to minimize the effects of input polarization [7]. Here, the polarization dependency of an SMS fiber structure is studied theoretically and experimentally.

The effect of temperature on the optical and mechanical properties of silica could affect the performance of fiber-based edge filters. Therefore, it has a significant influence on the accuracy of wavelength measurement. A research has

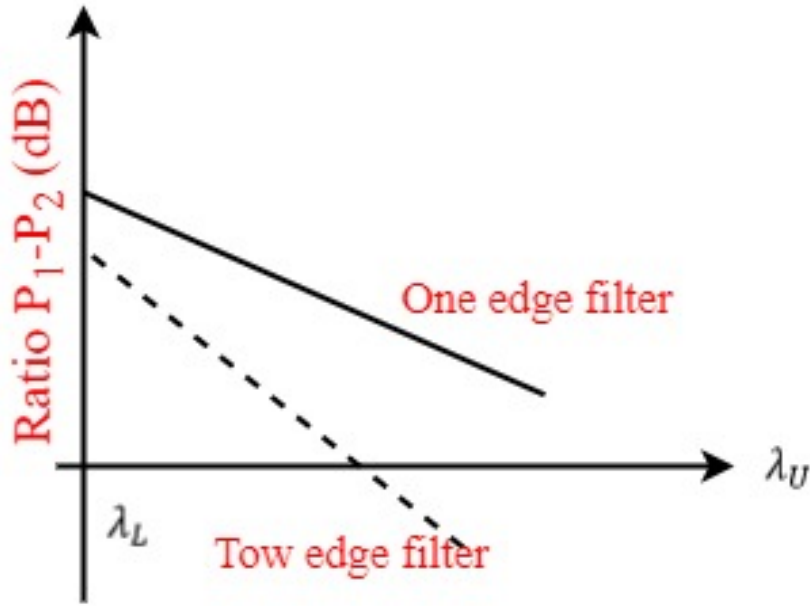


Figure 1.11

been done [14] on the peak wavelength shift of the transmission spectral response of an SMS fiber structure due to temperature change and the reduction of this peak shift to a low value by a temperature compensation scheme. However, in an edge filter-based ratio metric wavelength measurement scheme, even slight peak wavelength shift can induce enough ratio variation to degrade wavelength measurement accuracy [8]. Thus, a research about the effect of temperature on SMS-based edge filter is required to implement a suitable temperature compensation scheme.

1.5 Sensing applications of SMS fiber structures

As an alternative to FBG sensors, SMS fiber can be exploited as temperature and strain sensors with the low cost and simple production advantages compared to FBGs. SMS fiber sensors can be evaluated in different ways, for example by tracking the peak wavelength or by dipping in the spectral response using an optical spectrum analyzer (OSA) or by tracking the position of an edge in the SMS spectral response using a ratio metric intensity measurement system. The temperature or strain measurement techniques required the use of an OSA which

is costly and low speed.

In this text, SMS fiber sensors in an intensity measurement scheme utilizing ratio metric power measurement are studied, offering low cost, simple configuration with higher speed measurement compared to sensors which employ an OSA.

1.6 Effect of misalignment on an SMS

The application of SMS fiber as edge filters for wavelength measurement requires further study of several issues relating to the effect of misalignment of SMS fiber cores, polarization dependence and temperature dependence. The effect of misalignment of the SMS fiber cores, during the production process, on the spectral responses of X-type edge filters is studied. A commercial fiber splicer is commonly used to splice SMF to SMF or MMF to MMF with very low loss as well as low lateral core offsets [42]. However, fusion splicers are not pre-programmed to deal with splicing SMF to MMF therefore significant lateral core offset errors may arise during the splicing process for SMF to MMF or vice-versa. If lateral core offsets exist, the MPA based on LP_{0m} cannot be used since it is not a perfect alignment between the axes of the fibers. As a result, to study the effect of misalignment of SMS fiber using an MPA, it is necessary to calculate all possible modes in the MMF section and not only the LP_{0m} modes.

A numerical model based on the MPA using the finite difference method (FDM) was developed to study the effect of misalignment of SMS fiber cores. It was found that a limit of tolerable misalignment of SMS fiber cores exists beyond which the spectral performance of the edge filter-based SMS fiber structure degrades unacceptably. The experimental verification of this result is also presented.

1.7 Misalignment limits for a singlemode-multimodesing fiber-based edge filter

Misalignment effects on the spectral characteristics of edge filters based on singlemode-multimode-singlemode (SMS) fiber structures are investigated numerically and experimentally. A modal propagation analysis is used with a set of guided modes calculated using the finite difference method (FDM) to determine the transmission loss of the SMS-based edge filters. A limit for the tolerable misalignment of the SMS fiber-based edge filter is proposed, beyond which the spectral performance of the SMS structure degrades unacceptably. The numerical results are verified experimentally with good agreement.

Singlemode-multimode-singlemode (SMS) fiber structures have been investigated for use in several applications e.g. as a refractometer, a bandpass filter, and an edge filter [40]-[1]. An optical device based on the SMS fiber structure offers an all-fiber solution for optical communications and optical sensing applications with the advantages of simplicity of packaging and ease of inter-connection to other optical fibers.

The SMS structure is fabricated by splicing a precisely dimensioned multimode fiber (MMF) section between two singlemode fibers (SMFs). Ideally, the centre axes of all the fiber cores are precisely aligned. However, in practice the splicing process itself, along with the manufacturing variations in corecladding concentricity can introduce lateral misalignment between the centres of the SMF-MMF-SMF cores.

In the ref. [37], [1], and [23], the SMS fiber structure is analyzed using a modal propagation analysis (MPA) for the linearly polarized (or scalar) modes. The input light can be assumed to have the field distribution of the fundamental mode of the SMF (LP)

[59]. When the light launches into the MMF, the input field can be decomposed into the eigenmodes(LP_{nm}) of the MMF. Due to the circular symmetric nature of the input field and an ideal alignment assumption, the number of guided modes of the MMF used in the modal propagation analysis is greatly reduced from to or the circular symmetry modes. This reduced number of modes means

the calculation can be performed efficiently. In LP_{nm} to LP_{0m} [40] and [41], the SMS structure is investigated using the beam propagation method, where it is assumed that only the circular symmetry modes exist. With this assumption the optical field is simplified so that it is independent of the angular coordinate in a cylindrical coordinate system. However, if the centre (or meridional) axes of the SMS cores are misaligned relative to one another, it cannot be assumed circularly symmetrical modes. Thus, both approaches published so far cannot be used to study the effect of misalignment in an SMS structure.

An MPA using a complete set of hybrid modes or vectorial form guided modes in the MMF has been proposed to analyze the misalignment effect [10]. In this approach, a complete set of guided modes in the MMF is calculated and an adaptive algorithm is developed to perform mode expansion of the optical field in the MMF. However, the complete set of guided modes in the MMF can also be solved with an alternative numerical method, the finite difference method (FDM) [61]. The numerical approach using FDM offers simplicity of its implementation. In this paper, the FDM is used to calculate the complete set of guided modes in the MMF and then the MPA was performed to analyze the misalignment effect. Building on previous research on an SMS-based edge filter [41], [1], in this paper, the effect of fiber misalignment within an SMS-based edge filter was investigated both numerically and experimentally, so as to establish an upper limit on tolerable misalignment above which the performance of SMS structure has degraded significantly.

To put the misalignment induced performance degradation in context, the application chosen here for the SMS was that of an edge filter used within a ratiometric wavelength measurement system. A ratiometric wavelength measurement usually consists of a 3 dB coupler with the two outputs connected to an edge filter arm with a well defined spectral response and a reference arm, or alternatively two edge filters arms with opposite slope spectral responses can be used. The use of two opposite slope edge filters can increase the usable resolution of the ratiometric system [29]. A ratiometric wavelength measurement-based system on two opposite slope SMS-based edge filters was built and demonstrated in this paper.

1.8 SMS-based edge filters

A schematic structure for a ratiometric wavelength measurement consisting of two SMS-based edge filters is shown in Fig. 1.12. The target spectral responses in dB of the SMS-based edge filters are shown in the Fig. 1.13, and can have either a negative (P1) or a positive (P2) slope. Two key parameters for an edge filter are baseline loss and discrimination range. The SMS-based edge filter operates over a wavelength range from λ_1 to λ_2 with a progressively larger or smaller transmission loss as the wavelength increases from λ_1 to λ_2 , for the negative or positive slope, respectively. The baseline loss is defined as the transmission loss of the filter at λ_1 or λ_2 , for the negative and the positive slope, respectively, while the discrimination range is the difference between the transmission loss at λ_1 and λ_2 . The corresponding ratio (P2-P1) of the two outputs over the wavelength range is presented in the Fig. 1.14. The wavelength of an input signal can be determined through measuring the power ratio of the output ports at the outputs of the two arms, assuming a suitable calibration has taken place.

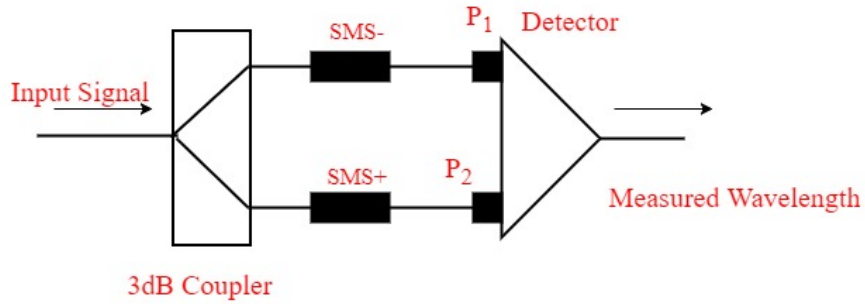


Figure 1.12

The fiber structure under consideration consists of an input SMF, a sandwiched MMF section, and an output SMF, as shown in Fig. 1.15. The concentric alignment and misalignment conditions in the Cartesian coordinate system, between the input SMF, MMF section, and output SMF cores, are shown in Fig. 1.16 and 1.17, respectively. The radii of SMF and MMF are denoted as R_s and R_m , respectively. The input SMF and output SMF positions are denoted by the coordinates and $I[x, y]$ and $O[x, y]$ respectively, where x and y are in μm .

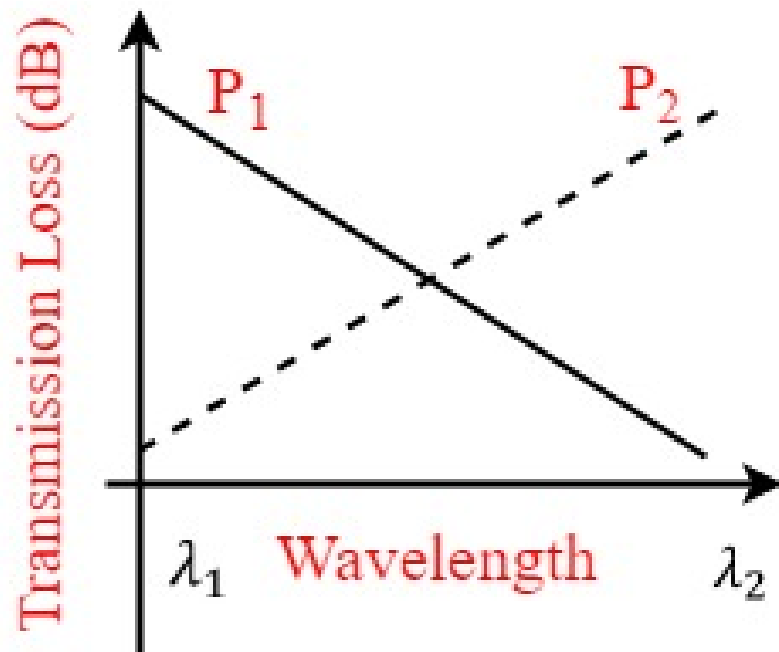


Figure 1.13

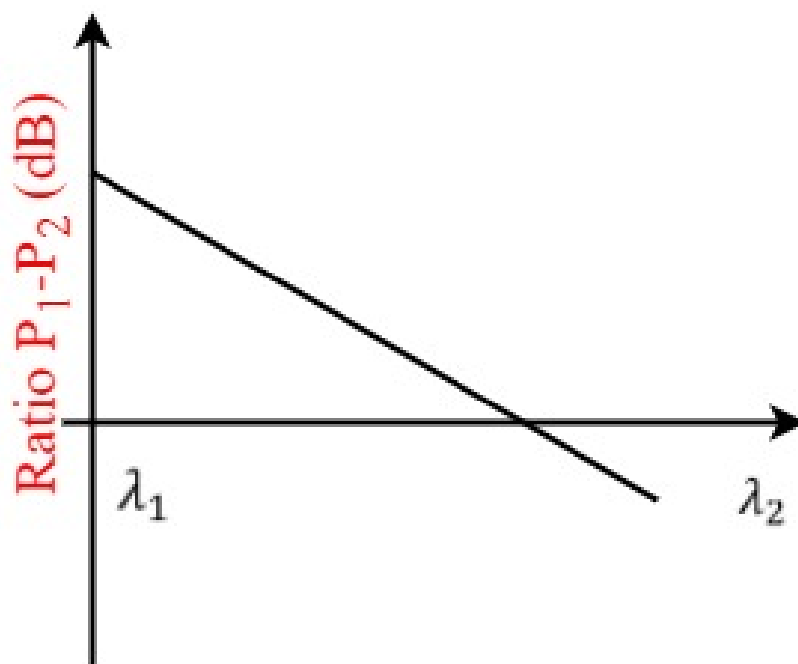


Figure 1.14

Single mode Fiber | Multi Mode | Single mode Fiber

→
Z axis : propagation direction

Figure 1.15

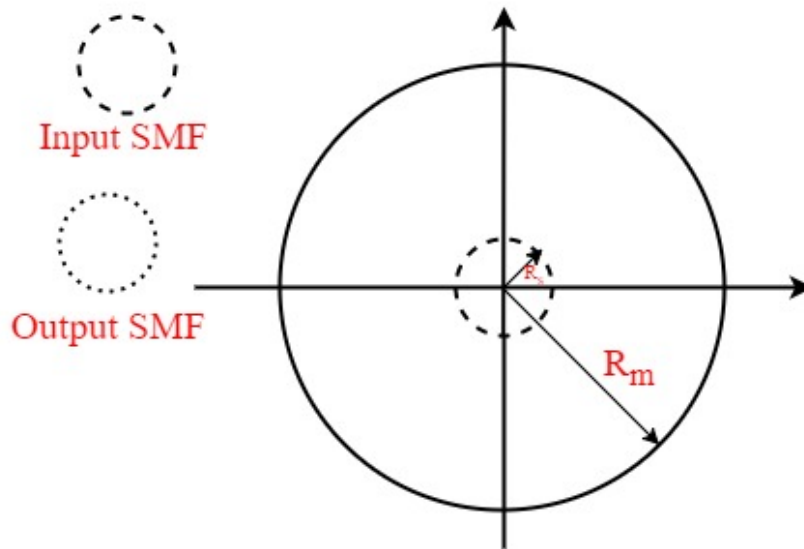


Figure 1.16

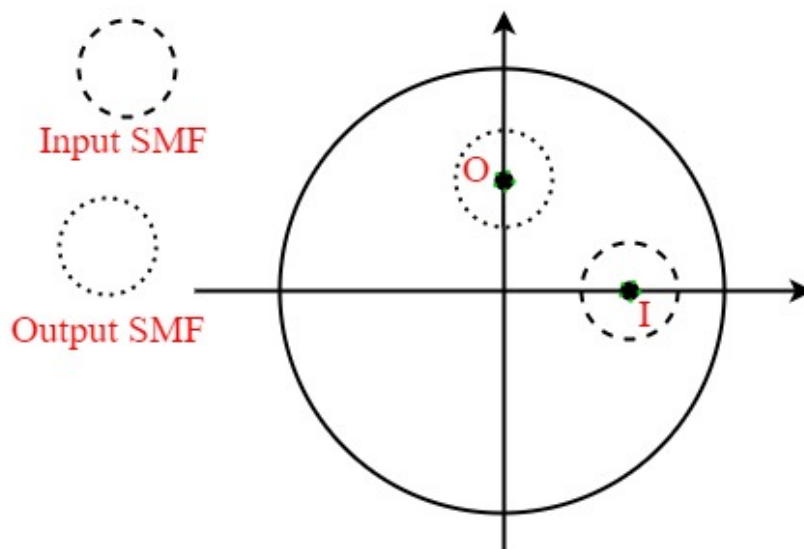


Figure 1.17

1.9 Modal propagation analysis

The MMF section can support many guided modes and the input field is reproduced as single image at periodic intervals along the propagation direction due to the interference between these guided modes. This is the so-called selfimaging principle and the distance at which self-imaging occurs is called the reimaging distance. The approach used here to analyze the field distribution in the MMF section is a modal propagation analysis [33]. In the MMF, an MPA using a cylindrical coordinate system has been employed in [37], [1], and [23] based on a scalar approximation of the LP_{0m} modes. The LP_{0m} modes could not be used to investigate misalignment effects because it only consists of circularly symmetrical modes. To analyze misalignment it is necessary to calculate a complete set of guided modes in the MMF LP0m LP0m [10]. In the approach used here, the MPA is performed in the Cartesian coordinate system with a set of calculated guided modes using FDM to allow investigation of misalignment effects.

The MPA procedure is as follows: the input light is assumed to have the field distribution $\psi(x, y, 0)$ of the fundamental mode of the SMF. The input field can be decomposed into the eigenmodes of the MMF, $\phi_v(x, y)$ when the light enters the MMF section. The input field at the MMF can be written as:

$$\psi(x, y, 0) = \sum_v c_v \phi_v(x, y) \quad (1.5)$$

where c_v is the excitation coefficient of each mode. The c_v coefficient can be calculated by an overlap integral between $\psi(x, y, 0)$ and $\phi_v(x, y)$

$$c_v = \frac{\int \psi(x, y, 0) \phi_v(x, y) dx dy}{\sqrt{\int \phi_v^2(x, y) dx dy}} \quad (1.6)$$

As the light propagates in the MMF section, the field at a propagation distance z can be calculated by

$$\psi(x, y, z) = \sum_v c_v \phi_v(x, y) \exp(j\beta_v z) \quad (1.7)$$

where β_v is the propagation constant of each eigenmode of the MMF. The transmission loss in dB can be determined by using the overlap integral method between $\psi(x, y, z)$ and the eigenmode of the output SMF $\psi_0(x, y)$

$$L_s(z) = 10 \cdot \log_{10} \left(\frac{|\int \psi(x, y, z) \psi_0(x, y) dx dy|^2}{\int |\psi(x, y, z)|^2 dx dy \int |\psi_0(x, y)|^2 dx dy} \right) \quad (1.8)$$

Here $\phi_v(x, y)$ and β_v can be obtained by using a semi-vectorial FDM. It should be noted that FDM calculates a set of all possible guided modes in the MMF section, not just concentric circular modes, allowing the transmission loss due to misalignment to be calculated. Using the above equations, the light propagation in the whole structure can be analyzed.

1.10 Design example and spectral response

To investigate the effect of misalignment, in the first instance it is necessary to present a typical SMS structure designed to meet a target spectral response and calculate its ideal, perfectly aligned, spectral response.

To design the SMS-based edge filter, the MMF length needs to be determined. It has been shown that the re-imaging distance is wavelength dependent [37], [23]. If re-coupling into the output SMF takes place at the reimaging distance, then the MMF section of the SMS structure has by definition a length equal to the re-coupling distance and operates as a bandpass filter as in [37] and [?]. However, for the purpose of designing an edge filter, the bandpass response can be considered as two spectral responses, on the either side of a centre wavelength. Consequently, the device can behave as an edge filter for a selected wavelength range. Two SMS-based edge filters with opposite slope spectral responses within a given wavelength range can be obtained by choosing two bandpass filters with appropriate centre wavelengths [1].

As an example, to illustrate the design process, a target wavelength range for wavelength measurement from $\lambda_1 = 1520$ nm to $\lambda_2 = 1545$ nm was chosen. This range is chosen as it corresponds to the typical centre wavelengths for many fiber Bragg grating (FBG) sensors. Based on the target spectral responses as in Fig. 1.13, the SMS-based edge filters are designed with the baseline loss ζ -8 dB and the desired discrimination range ζ 8 dB. A standard SMF28 fiber was chosen as the SMF, for which the parameters are: the refractive indices for the core and cladding are 1.4504 and 1.4447 respectively (at a wavelength of 1550

nm), and the radius of the core $R_s = 4.15 \mu\text{m}$. An MMF type AFS105/125Y was chosen as the MMF section for which the parameters are: refractive indices for the core and cladding are 1.4446 and 1.4271, respectively, with a core radius $R_m = 52.5 \mu\text{m}$. The small difference between the refractive indices of the SMF and MMF means that the Fresnel reflection occurring at their interface is negligible (the level of reflection is -54 dB or lower relative to the injected light level) and a one-way modal propagation analysis can be used RS Rm [59]. As mentioned above, for the specified wavelength range, two opposite response slope edge filters (negative and positive slopes) can be obtained by designing two bandpass filters with peak wavelengths: $\leq 1520 \text{ nm}$ and $\geq 1545 \text{ nm}$, respectively. From (10) in ref [23], the peak wavelengths from 1500 to 1520 nm correspond to the MMF lengths $L = 44.25$ to 43.66 mm , and from 1545 to 1560 nm correspond to $L = 43.00$ to 42.58 mm . Suitable peak wavelengths for the targeted wavelength range are 1510 and 1547 nm and the corresponding MMF lengths are $L = 43.96 \text{ mm}$ and $L = 42.95 \text{ mm}$, for the negative and positive slope edge filters, respectively. The peak wavelengths at 1510 and 1547 nm were chosen for the SMS-based edge filters because their transmission loss responses have a suitable spectral response over the targeted wavelength range from 1520 to 1545 nm. The transmission loss responses, calculated using (3.4) for the designed SMS-based edge filter, are shown in Fig. 1.18. These responses represent the performance of the design example for the case of perfect alignment. It can be seen that the two opposite edge filter responses within the targeted wavelength range can be achieved using two bandpass filters. The calculated negative and positive slope responses of the SMS-based edge filters from 1520 to 1545 nm have a transmission loss from -7.20 to -15.53 dB and -11.84 to -0.77 dB, respectively, and the corresponding discrimination ranges are 8.33 dB and 11.06 dB, respectively, suitable for use as edge filters.

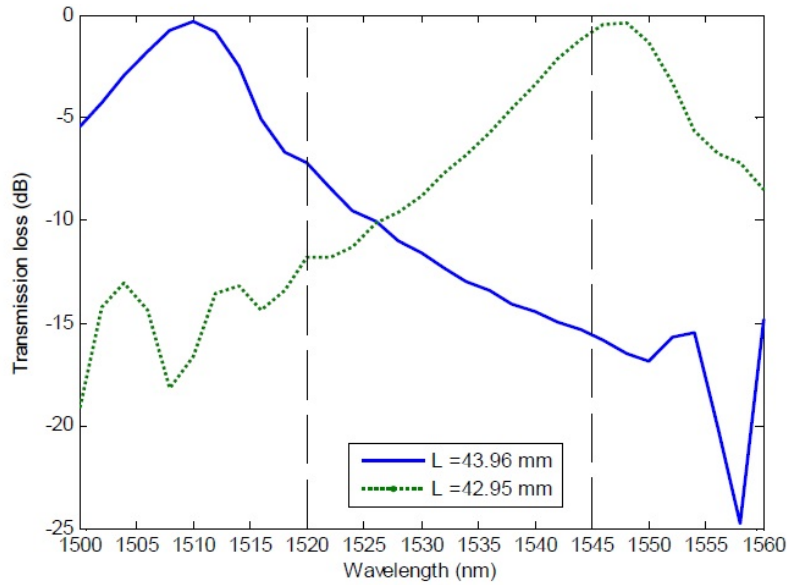


Figure 1.18

1.11 Temperature effect on SMS sensors (BIF as sample)

Among different sort of fiber sensors, Single mode-Multimode - Single mode (SMS) optical fiber sensors have gained great consideration in the recent years since they are easy to install and low in cost. A SMS sensor is composed of a short section of multimode (MM) fiber spliced between two single mode (SM) fibers; figure 1.19

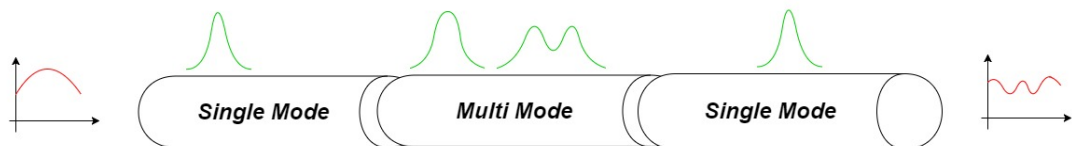


Figure 1.19

In SMS structure, the multimode section propagates the light modes with different phase velocities therefore an interference pattern is formed at the MM-SM junction which is based on the phase shift obtained in the MM section. Hence in SM section of receiver side the power value is changed. Since the phase shift in the MM section is affected by perturbations along the propagation length (de-

pending on MM section length, refractive index and temperature)the can explain the drop in the received power.

in the simple case where there are only two modes excited in MM section and polarization conversion effects are disregarded, the output power of the SMS structure on the fundamental mode will be expressed as a Mach-Zehnder interferometer:

$$P_{out} \propto P_{in}(1 + \Psi^2 + 2\Psi \cos \varphi) \quad (1.9)$$

Where P_{in} and P_{out} are the input and output power respectively, Ψ is a coefficient based on the combination of the two modes and φ is the phase difference which depends on the interaction length and the wavelength. If the broadband light is inserted in the SMS structure the output spectrum will display spectral fringes figure 1.19, whose free spectral range (FSR) is approximated by:

$$FSR \simeq \frac{\lambda^2}{2\Delta L \Delta n_{eff,01-11}} \quad (1.10)$$

where ΔL is the length of the MM section, $\Delta n_{eff,01-11}$ is the difference of effective refractive index between the two modes and λ is the central wavelength at which the spectral fringes are observed [18].

The SMS structure is used to produce various types of sensors. for instance the main and most successful quantities measured by a SMS sensor for fiber Bragg gratings have been refractive index [26], temperature [31] and displacement [12].Considering that any interferometric sensor is sensitive to different physical quantities which may leads to misreading and systematic errors. There are couple of solutions to deal with this problem. For instance, using a pair of SMS sensors in a ratiometric power scheme has compensated the cross sensitivity of strain and temperature [2].Some studies have been done on combining SMS sensors with FBGs since the SMS structure displays red shift to temperature and blue shift in strain while FBG displays a red shift to both temperature and strain[6], [4].

Many investigations has been done over the ways to produce modal interference in an optical fiber. Some have used A short section of MM fiber [21],[2],[11] and others used coreless fiber [31],[4]. However some publications have showed by down-tapering two closely spaced sections of a SM fiber it is possible to make an

in-line Mach-Zehnder interferometer [19],[35]. The recent publications [13],[34] shows a single taper acts as an interferometer between the core and cladding modes hence it can be used as an interferometric sensor which is sensitive to the environment. Four important features of SMS sensors are listed for a review:

- SMS are interferometric sensors so they are not sensitive to the power fluctuations within the interrogation scheme.
- SMS sensors show higher sensitivity than FBGs in general
- SMS prototypes are easily made using conventional fusion splicers which are accessible in any fiber optics facility so they do not require any specialized equipment.
- etching process is not necessary in most of the cases since SMS sensors can be utilized for specific sensing applications simply by coating with proper materials.

While SMS sensors seem to be a simple and effective alternative to FBGs, it should also be mentioned that multiplexing a large number of sensors on the same fiber can be complex, hence SMS sensors are not suitable for large sensor networks.

In order to reduce the complexity of constructing SMS sensors and to review new designs, we studied the bend insensitive fiber as a replacement for the common MM section of the SMS structure. Bend insensitive fibers (BIFs) are telecom-devised SM fibers that are more applied in fiber-to-the-home (FTTH) networks, because they have lower bending loss than conventional SM fibers while preserving the compatibility with them to some extent (i.e., they can be spliced to SM using the same equipment and display similar optical features such as mode field diameter). By proper design of the refractive index profile it is possible to produce a tighter confinement of the optical signals into the core of the BIF. The drawback of BIFs is that around the 1300 nm, they operate close to the cut-off of the LP_{11} mode which is the first higher order mode (HOM), and therefore the propagation could be supported for several meters. The discontinuities in the propagation path caused by slightly misaligned splices, induce the transfer of

some of the optical power associated with the fundamental LP_{01} mode into the LP_{11} mode. The two modes can interfere coherently since the coherence length of the source is often longer than the separation between the discontinuities and the transverse intensity pattern becomes sensitive to any spurious effect such as vibrations and thermal drifts that may waggle the phase of each mode. The spatial instability of the field distribution leads to a low-frequency intensity noise at the receiver, which causes the Multipath Interference (MPI) penalty in telecom applications. This phenomenon is extensively studied in [17], [15], resulting that MPI detrimental levels can happen in short misaligned BIF sections. Then we improvised to use the multimodal propagation in BIFs as means for optical fiber sensing and fabricated a single mode fiber (SMF) BIF SMF structure that proved to be sensitive to temperature.

1.12 SMF-BIF-SMF Sensor Setup

Schematic of Fig 1.20 a 3 cm long commercial BIF (compliant to ITU-T Recommendations G.657) was spliced at both ends to commercial SM fiber pigtailed (compliant to ITU-T Recommendations G.652) with a radial offset of $5 \mu m$ which is a large offset selected to maximize the MPI effect, exactly the opposite of what happens in telecommunication applications, and therefore enhance the spectral oscillations due to the interference between the modes excited in the MM section when coupling back to the SM receiver side. The misaligned BIF jumper implies about 0.8 dB loss, which is negligible since the sensing functionality (based on the shift of the spectral response) is preserved.

Experimental results with various offset values have demonstrated that the selected value ensures a proper coupling between the fundamental and the first HOM. In fact, in MM section an infinite number of modes are excited by splicing. however, utilizing BIFs, which are single mode at the studied wavelength, the only coupling between the LP_{01} and the LP_{11} modes are relevant. This is distinctive feature of BIFs because it gives a very straightforward interference pattern and hence an outstanding advantage at the detector side.

The offset splices are created by a standard telecom arc fusion splicer driven

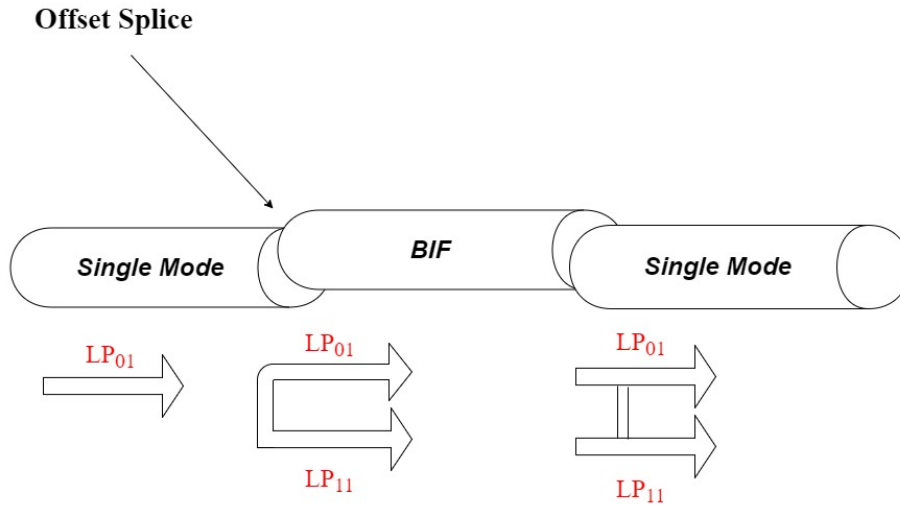


Figure 1.20

in manual mode and the fusion parameters are optimized for proper splicing. Literally, this is a quite long procedure since the power, the arc number and duration are tightly dependent on the type fiber and splicer machine. Normally splicers select the optimal parameters to produce an exact aligned splice automatically however in the studied case the splice was offset on purpose. Eventually it is required to reproduce the environmental parameters such as temperature, pressure, humidity precisely to ensure the same energy transfer during the splicing process. Some hints on splice optimization can be found in [43]. A picture of the obtained offset fusion splice is shown in Fig 1.21

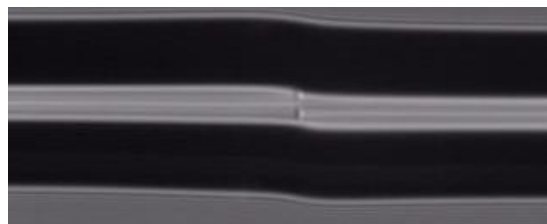


Figure 1.21

1.13 SMF-BIF-SMF Sensor Characterization

SMS sensor primary temperature response is achieved using a hotplate and a reference thermocouple Fig 1.22. The fiber sensor is placed and fixed on the

hotplate and to improve the thermal conductivity between the fiber and the metal plate a heat transfer compound is used. The pigtails of the sensors are connected to an optical spectrum analyzer as well as a broadband LED source which operates around 1300 nm. This wavelength was selected because at 1300 nm both the SMF and BIF are nominally in single mode conditions, however the attenuation for BIF first HOM is such that its contribution to power transfer when excited by the misaligned splice is not negligible. As a result at this wavelength the device acts as a two-mode interferometer. The temperature is swept between 22 ° C and 150 ° C and the correspondent spectra are achieved. The fiber sensor temperature is captured by the thermocouple. Fig 1.23 summarizes the results. We observe the shift of the spectral fringes toward longer wavelengths when the temperature increases.

The fringes visibility is around 2 to 5 dB and can be optimized further by manipulating the splices misalignment, BIF length and the light polarization. The latter effect, which has a key role in the evaluation of the MPI in telecommunication applications [36], will be completely studied in an ongoing measurement campaign. The free spectral range is measured about 12 nm. This value is compatible with that estimated by Eq. 1.10: the 3 cm long interference section and an estimated $\Delta n_{eff,01-11} \simeq 2.5 \cdot 10^{-3}$ predict a FSR of about 11 nm around $\lambda = 1300$ nm. The value of the effective refractive index difference $\Delta n_{eff,01-11} \simeq 2.5 \cdot 10^{-3}$ was estimated from the refractive index profile of the fiber computing the resonances on an equivalent radial transmission line problem [16].

The results define a monotonic relation between temperature and wavelength shift of interference fringes Fig 1.24, with a sensitivity of 55 pm=°C No remarkable hysteresis was observed in Fig 1.23 repeat the same spectral behavior when heated from 22 °C to 150 °C and then cooled back to the former temperature. The high sensitivity along with minor hysteresis made this sensor a good choice for many applications: for instance, to be used in monitoring the increment of temperature during thermo-therapies of solid tumors, such as laser ablation [27]. For this purpose, a smaller size SMS sensor should be examined, because the wider temperature range (40 °C/cm) require a distributed or semi-distributed temperature sensing platform. Multiplexed SMS sensors can make it happen ,

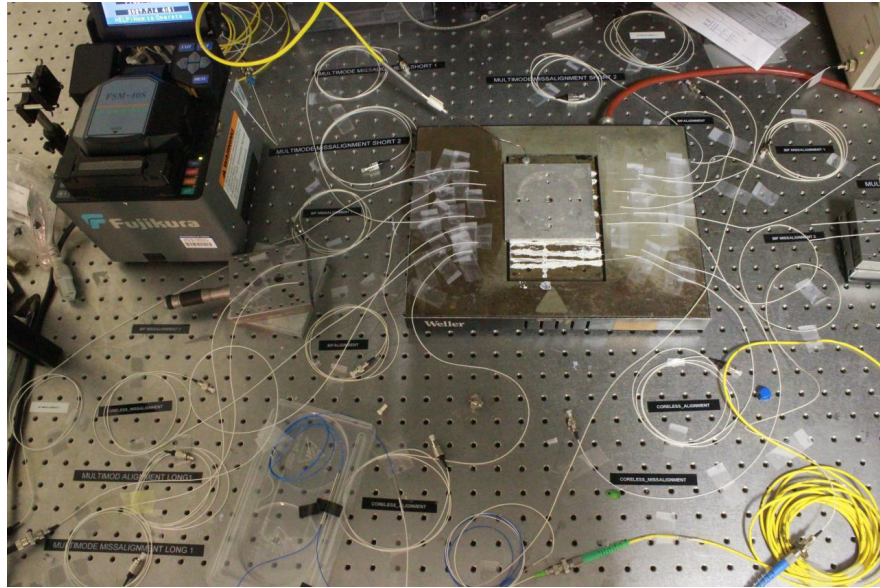


Figure 1.22

though some constraints on the number of sensing points would remain and the total performance should be evaluated precisely throughout extensive measurements with FBGs.

to summarize, one of the advantages of SMS fiber sensors is that the information is encoded in a wavelength shift. It is possible to compensate the sensor response for unwanted perturbations using some techniques to sort out the sensitivity to multiple parameters (e.g., temperature and strain). Furthermore, SMS sensors show opposite reaction to temperature and strain, making the compensation simple, for example by combining a SMS sensor with a FBG sensor. BIF sensors are applied in short-reach optical communication since they reflect low bending loss and are very effective in optical wiring of curbs and buildings. On the other hand, they propagate the first higher mode with low loss around 1300 nm, which can cause the undesired multipath interference effect. This behavior, undesirable in telecommunications, can be turned into a desirable feature for sensing applications. A short section of BIF, offset-spliced between two SM pigtaileds, can operate as a bimodal interferometric sensor. SMF-BIF-SMF sensor characterized as a temperature sensor. The temperature response remarked a sensitivity of $55 \text{ pm}/^\circ\text{C}$ and no hysteresis effects and a neat linear behavior. These findings are promising because they exhibit more sensitivity than common bare FBGs and even than typical SMS sensors.

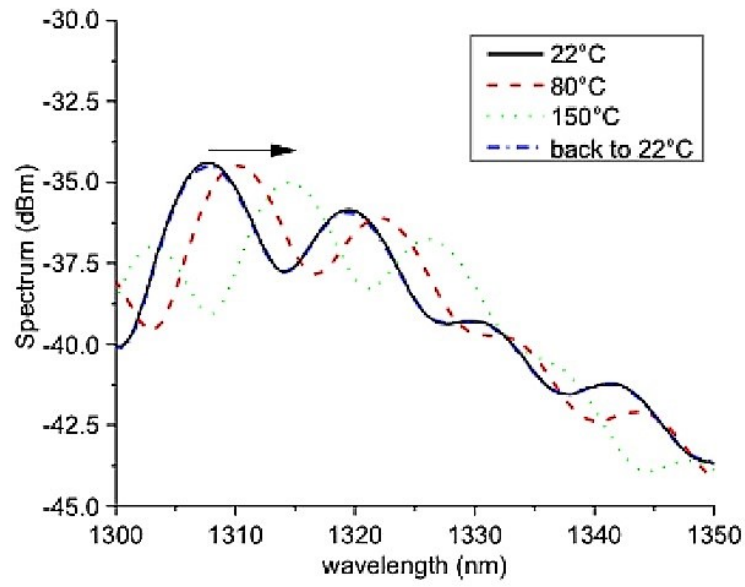


Figure 1.23

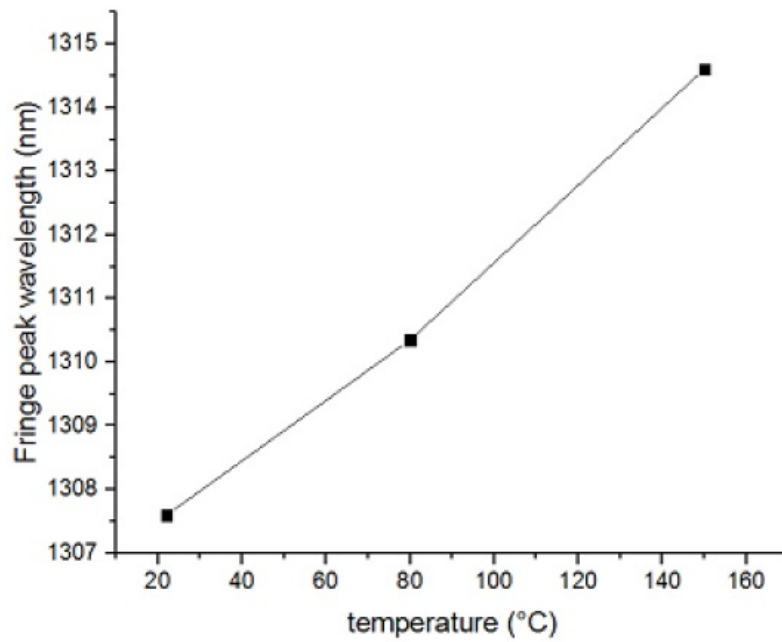


Figure 1.24

Chapter 2

Analyzing experimental result of temperature effect on various SMS sensors fiber

In this report, four different fiber sensor cases including SMS-BIF, SMS, SMS coreless and SMS SM2000 were studied and characterized in terms of wavelength variation and power amplitude inside a temperature range from room temperature $\approx 24^\circ\text{C}$ to 150°C with intervals of 5°C . In addition, we examined the effect of misaligned splice as well as aligned splice on the power spectrum for the above cases.

2.1 Framework

As depicted in figure 2.1, the experimental framework consist of an optical source, an Optical source Analyzer(OSA), a heater and a thermometer. The intended sensor fiber is connected to the source while it is placed over a heater, the other fiber sensor end goes to the OSA which itself connected to a PC to capture the results. To be precise in measuring temperature we exploit a separate thermometer which measures the heater temperature and send it to PC. To Observe the OSA and thermometer data on PC two different softwares were used respectively. It should be noted that the general experimental routine is to turn on the heater and for every 5°C interval record the power spectrum changes

observable through OSA. The numerical data results analysed in the software called OriginLab.

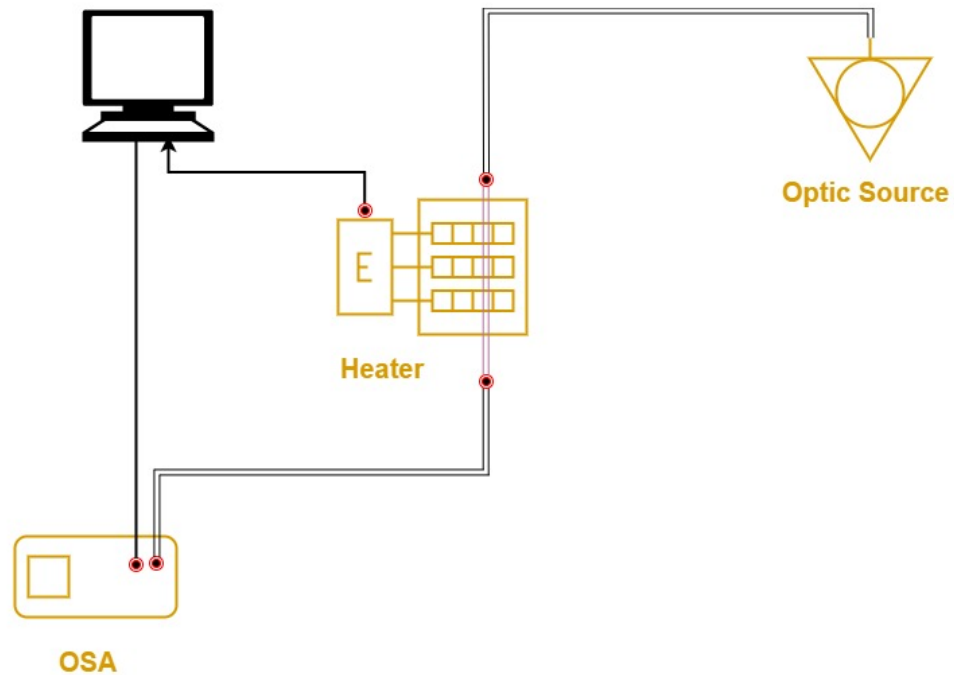


Figure 2.1: Framework

2.2 Producing SMS Fiber Sensor

The splicing process begins with the preparation for fiber's ends to be fused. It is required to strip all protective coating, jackets, tubes and strength members, just leaving the bare fiber showing. It is noted that the cables should be clean. Then using a fiber cleaver to only nick the fiber and then pull or flex it to cause a clean break rather than cut the fiber. The cleave end-face should be perfectly flat and perpendicular to the axis of the fiber for a proper splice. The last step is to fuse the fiber. When fusing the fiber, there are two important phases: aligning and melting. Since fiber optic splicer aligns two fiber ends automatically and that is not what we exactly looking for, we set the splicer in manual mode so that we can have either misalignment or full alignment. for misalignment cases splicer motor direction should be set on x axis and misalign the fibers for $5 \mu\text{m}$. Figure 2.3 and figure 2.4 depict the misaligned fibers inside the splicer.

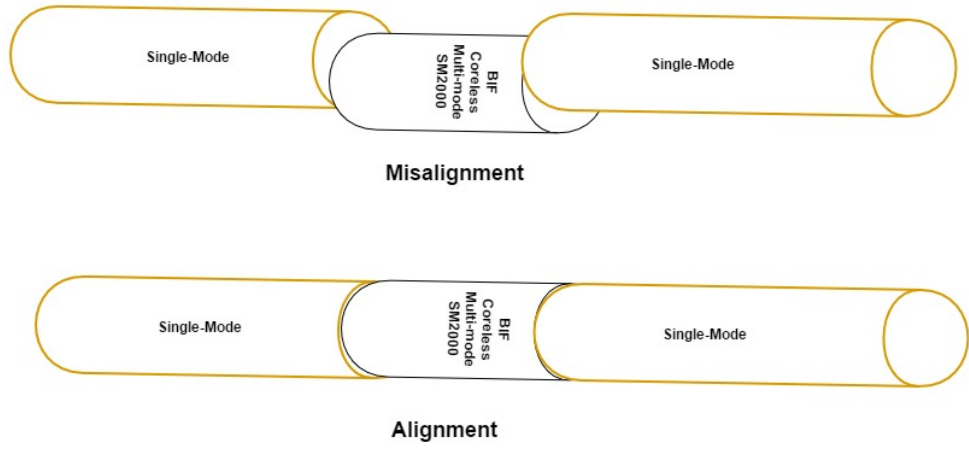


Figure 2.2: Misaligned SMS sensor fiber, Aligned SMS sensor fiber

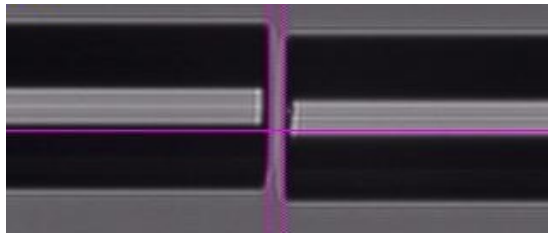


Figure 2.3: Misaligned fibers before splice

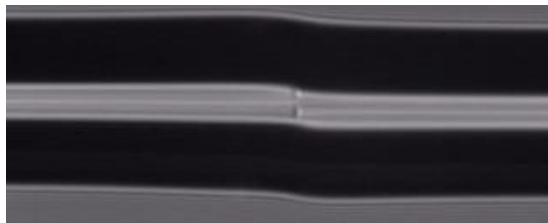


Figure 2.4: Misaligned splice

The same procedure is done for the full alignment except for the zero misalignment. Once proper or desirable alignment is achieved, utilizing an electrical arc to melt the fibers to permanently welding the two fiber ends together. Figure 2.5 and figure 2.6 depict the aligned fibers inside the splicer.

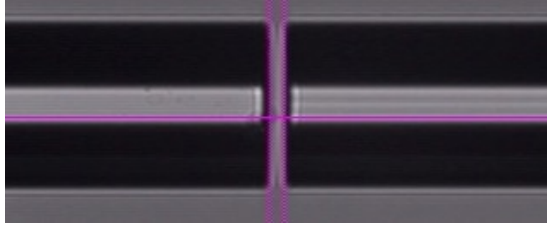


Figure 2.5: Aligned fibers before splice



Figure 2.6: Aligned splice

To produce SMS sensor, we detach a piece of fiber's core (in this experiment one of the types: BIF, coreless, multimode and SM2000) entirely from its coating and leave the core showing. Then each end of the fiber core is cut perpendicularly and spliced to two single mode fiber either in aligned state or misaligned.

2.3 SMS BIF

To begin we studied a sample model of SMS sensor which has a piece of Bend Insensitive single mode Fiber (BIF) in the middle. BIF is able to reduce bend loss sensitivity in comparison with a standard fibers. In this section we considered two sensors one in aligned state and one in misaligned state. according to the discussed framework 2.1 sensor is applied and the heater temperature is set to room temperature up to 150°C and record the results observable on OSA for intervals of 5°C . In the first sample of misaligned SMSBIF figure 2.7, 2.8 and 2.9 can be seen. Power spectrum affected by temperature increment. To investigate the changes we selected a peak and tried to follow the variation in power and wavelength.

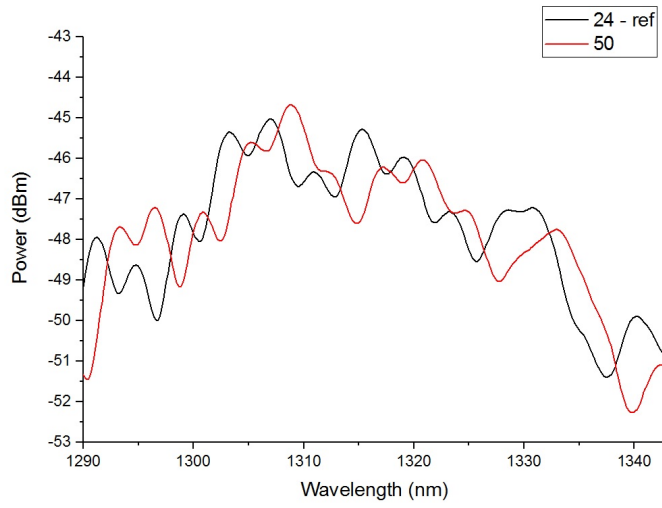


Figure 2.7

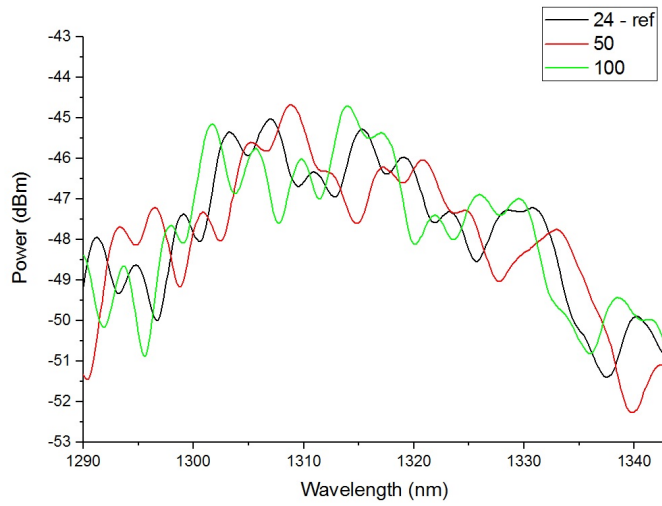


Figure 2.8

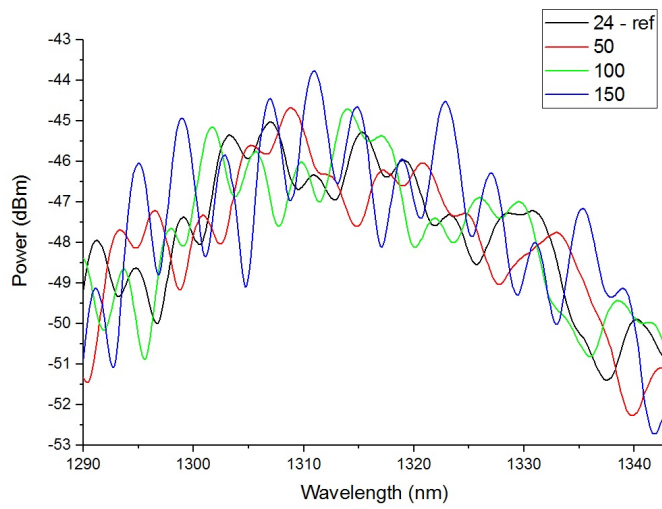


Figure 2.9

According to figure 2.10, by increasing the temperature power peak starts to decline and it falls from -45.31dBm to -47.95dBm. The power shift in this figure is 2.64dB. Figure 2.11 shows the peak shift over wavelength by temperature variations. In this sample where peak wavelength is 1315.4nm in room temperature reaches to 1331.4nm wavelength by increasing the temperature. Peak shift in this sample is 16nm and it has an incremental trend.

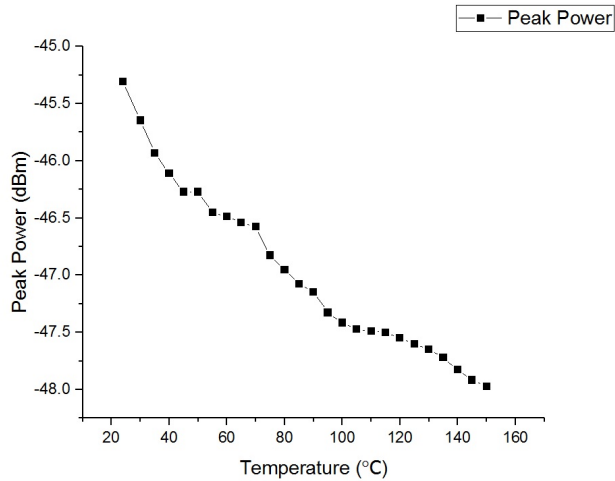


Figure 2.10

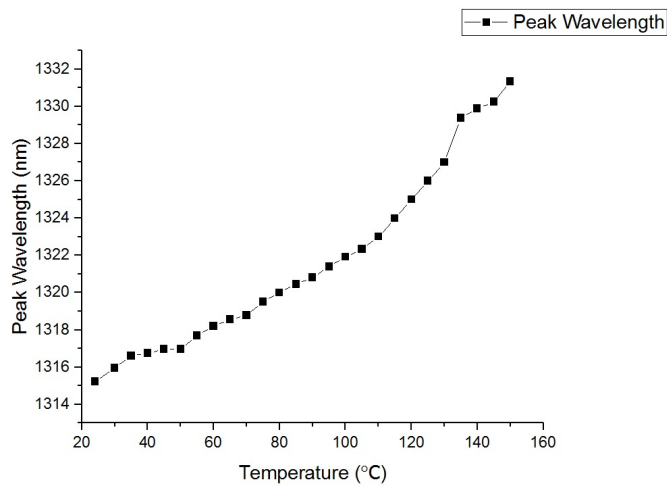


Figure 2.11

For the second sample, similar to first sample, figure 2.12 ,2.13, 2.14 and 2.15 show the power spectrum variation over temperature but the difference is here each of samples alone were compared to the sample taken in room temperature for a better perception on temperature effects.

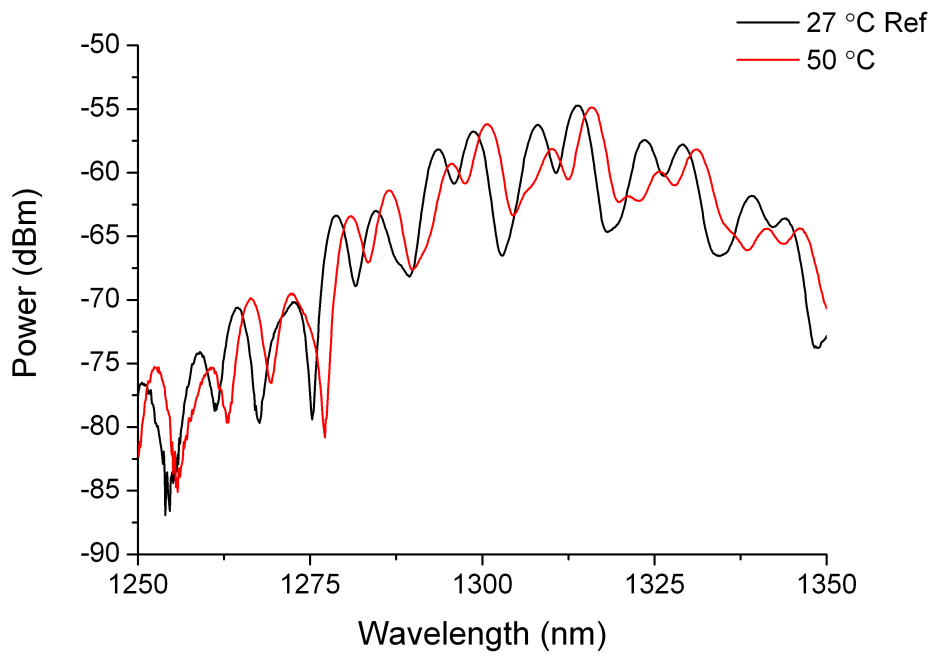


Figure 2.12

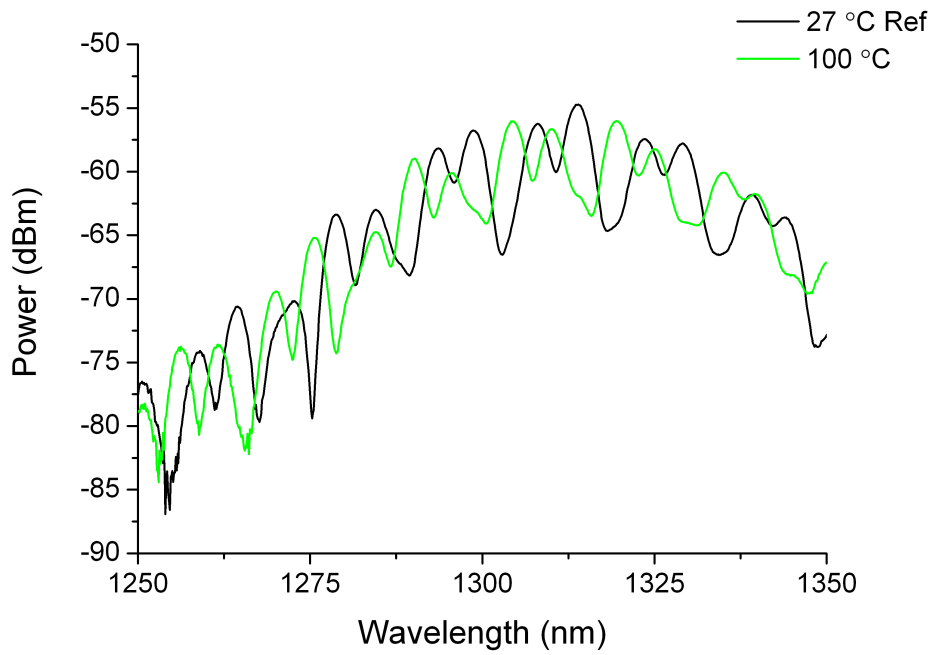


Figure 2.13

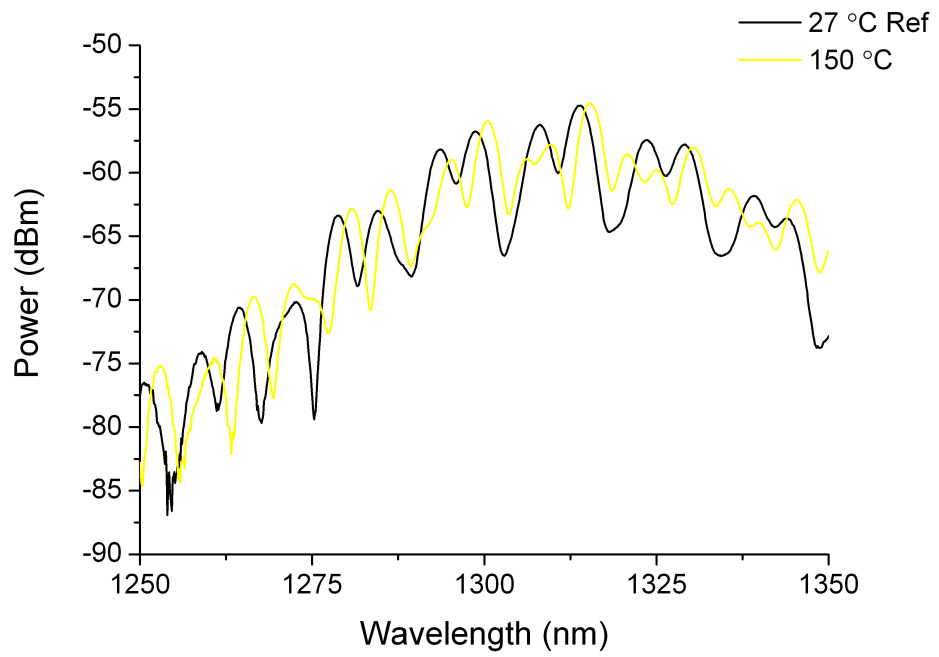


Figure 2.14

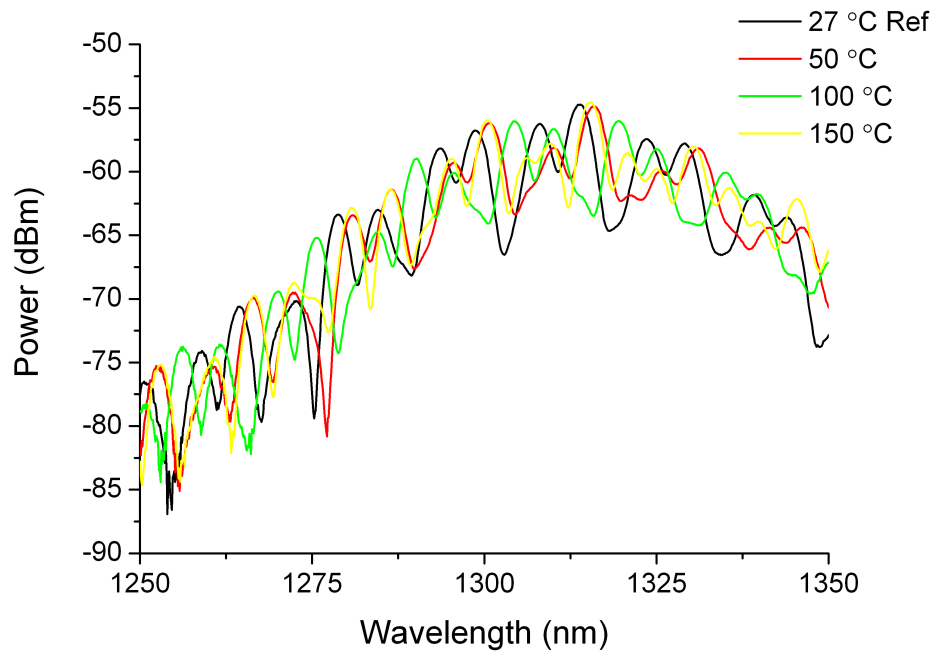


Figure 2.15

likewise, in this case by choosing a peak at power -54.7476345dBm and wavelength 1313.93554nm coordination, we measured the shift with temperature increment. In this sample wavelength changes is incremental and power changes is descending. at 150 ° C the peak position is at wavelength 1325.42283nm and power -60.0656416 dBm and power shift amount along power and wavelength axis 5.3180071dB and 11.48729nm respectively.

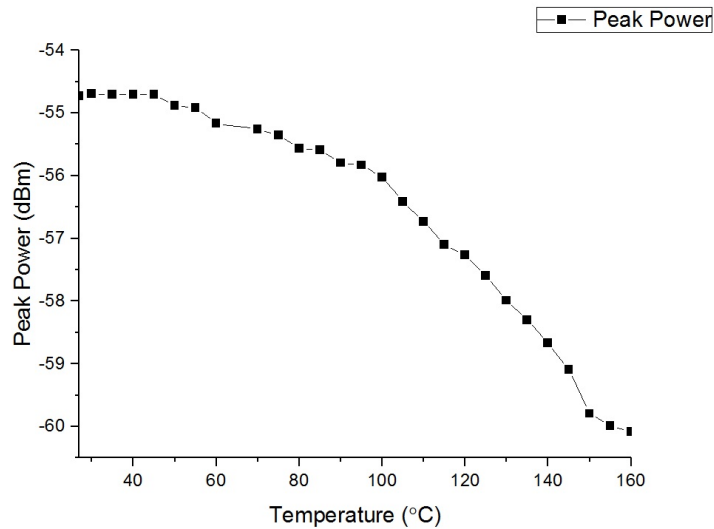


Figure 2.16

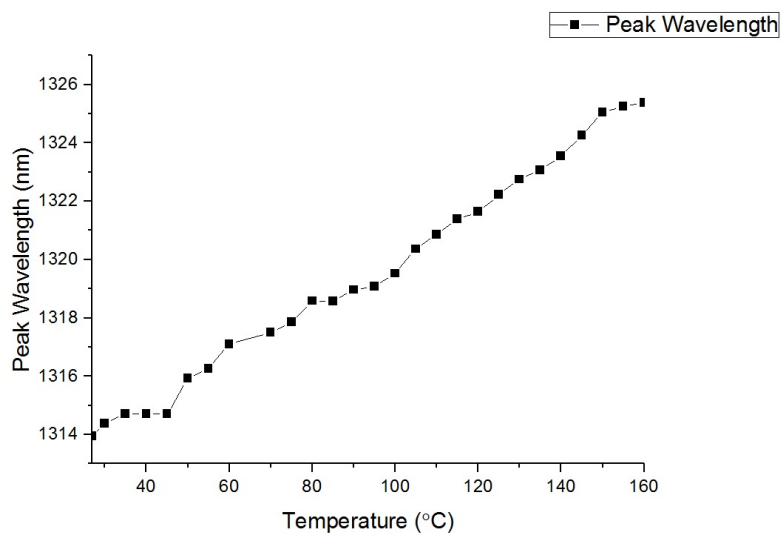


Figure 2.17

Now in a different experiment we study the SMS BIF in alignment state. As illustrated in figure 2.18 power spectrum has no notable changes over temperature

ranges from room temperature to 150 ° C and the curve is approximately fixed.

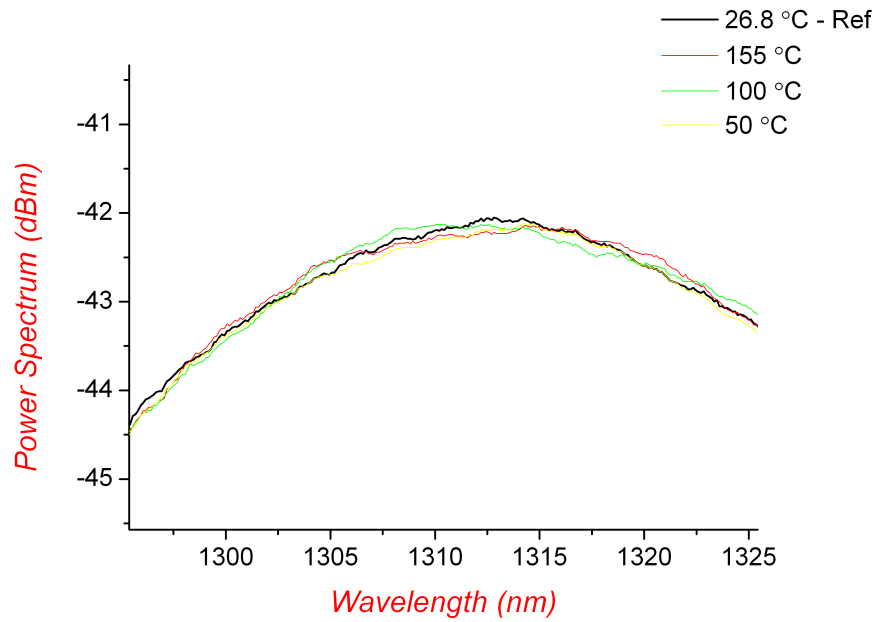


Figure 2.18

To be more precise on temperature effect on the peak position, figure 2.19 and figure 2.20 are considered. According to these two figures, increasing the temperature do not lead a shift in power peak neither in peak wavelength (they are almost fixed around -42dBm and 1314.25nm respectively).

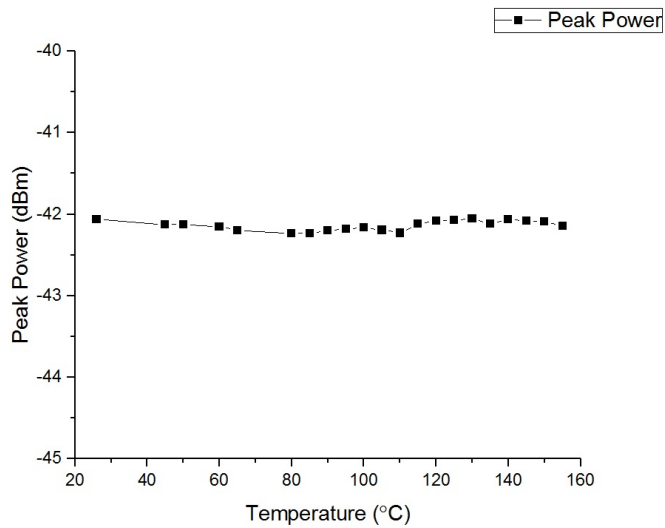


Figure 2.19

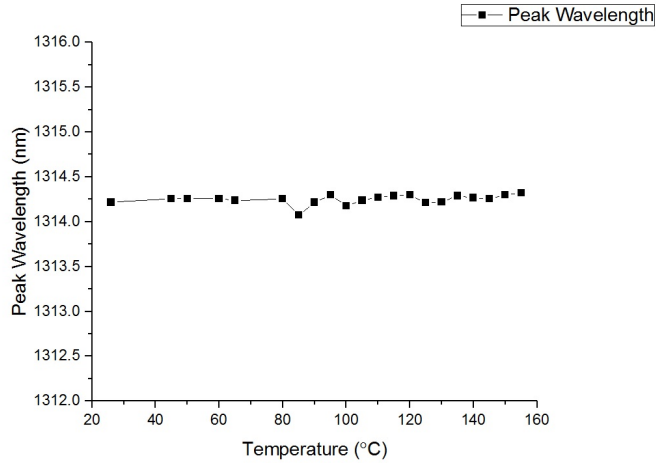


Figure 2.20

2.4 SMS Coreless Fiber

In this part BIF sensor replaced with coreless fiber and we apply SMS coreless which has been prepared in misaligned state into the framework 2.1 and increase the temperature from room temperature to 150 °C by the heater. The power spectrum variation were recorded for every 5 °C. Figure 2.21 illustrate the variation in four different temperature: room temperature 25.5 °, 50 °C, 100 °C, 150 °C. It is observable that power spectrum variation merely notable along power axis and wavelength variation is negligible.

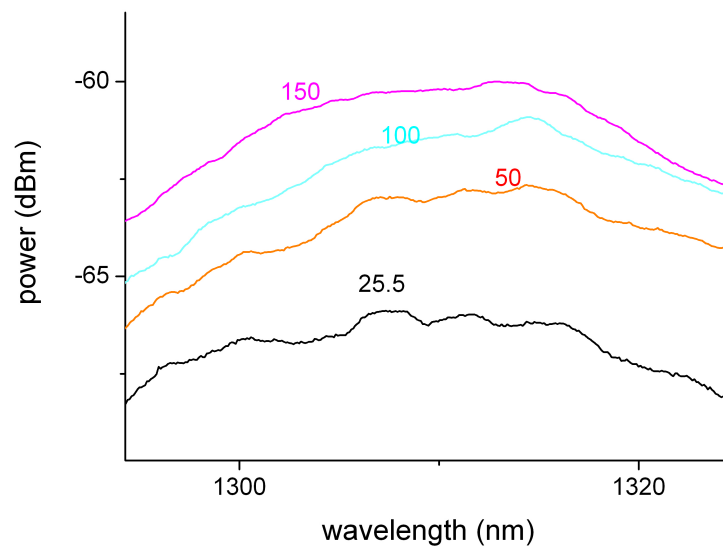


Figure 2.21

Figure 2.22 is in fact achieved by following a power peak in various temperatures. As it is observable, power is raised from -66.19dBm to -59.9dBm by increasing the temperature. The power shifted approximately 6.29dB in this sample.

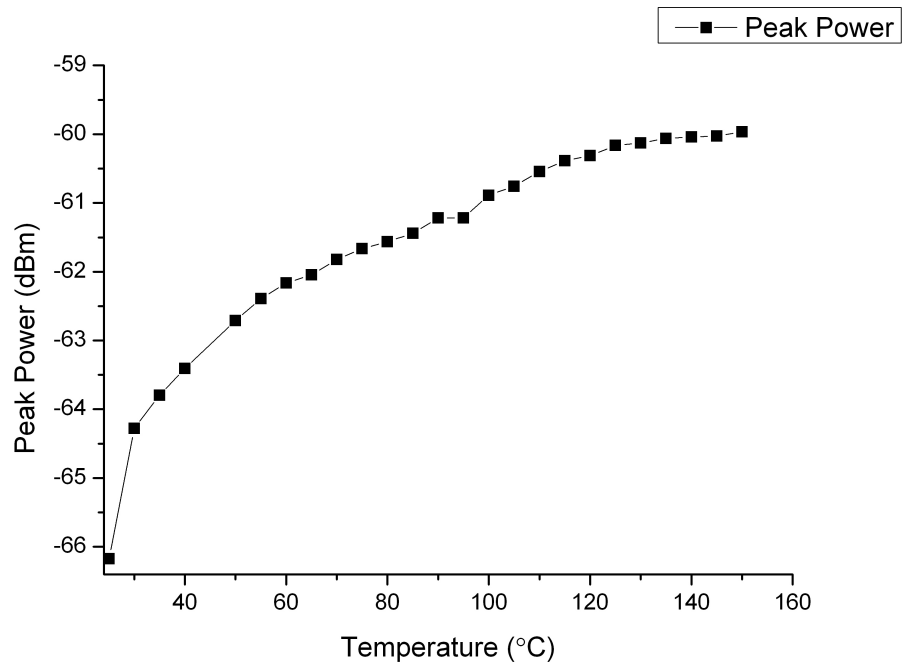


Figure 2.22

Figure 2.23 measures the peak position variation along the wavelength axis for different temperatures. As it is observable from this figure, the peak position is not varied along the wavelength axis and therefore there is no shift in this direction and the wavelength is fixed around 1315nm.

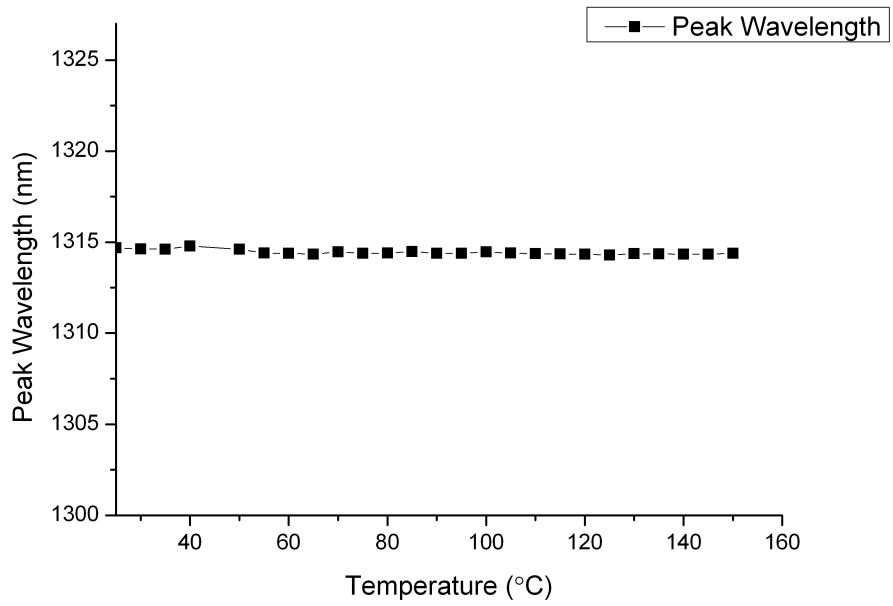


Figure 2.23

A notable point regarding this experiment is that the power spectrum curve after cooling down is not matching the reference power spectrum; by reference we mean the power spectrum figure before heating up the sensor. The peak variation is almost 1.5dB which is shown in figure 2.24.

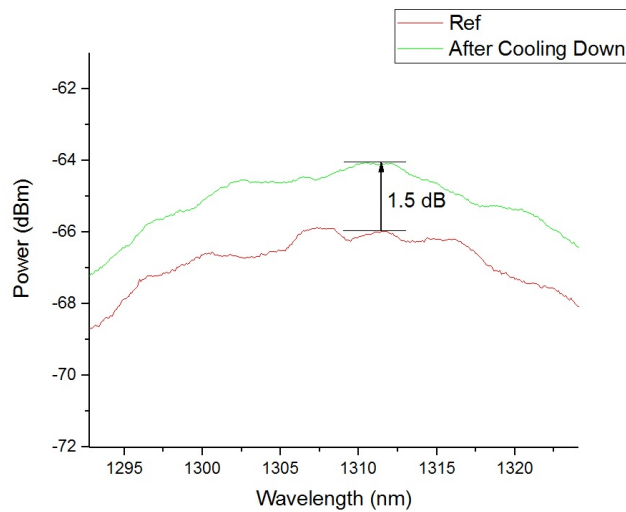


Figure 2.24

Likewise, we repeated the experiment for the coreless fiber sensor in aligned state. figure 2.25 shows the temperature effect on power spectrum peak.

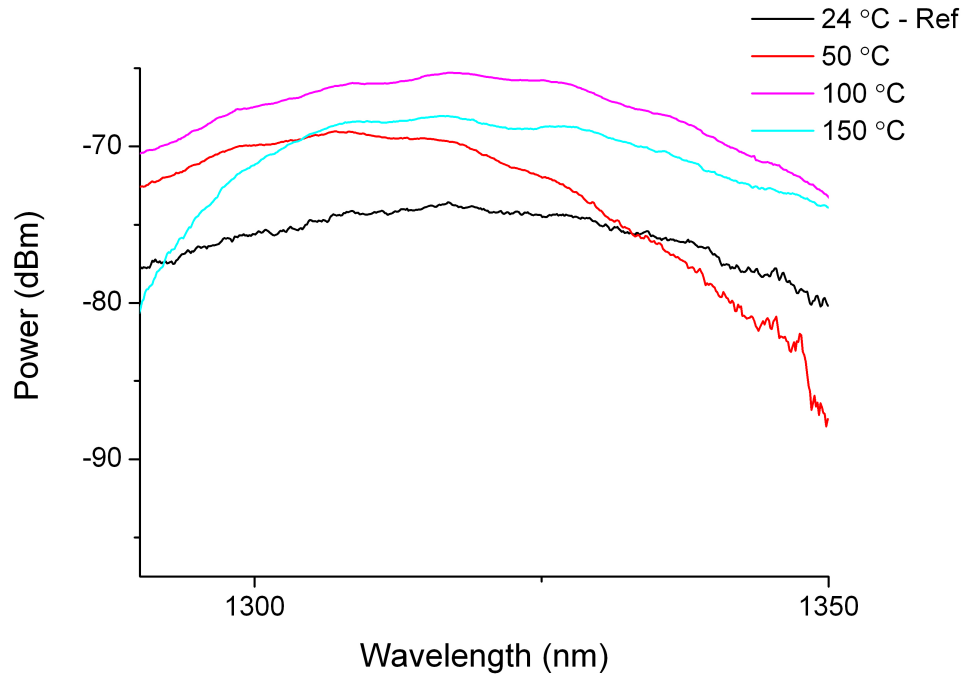


Figure 2.25

According to figure 2.26 the power peak does not have a regular and stable ascending or descending behavior. The power curve reaches the maximum at 105 °C. the difference of maximum amount (-65.18dBm) and the minimum amount (-73.6dBm) is almost 8.42dBm. However, this point slightly shifts along the wavelength axis by changing in temperature and it is almost placed around 1317.5nm. Figure 2.27.

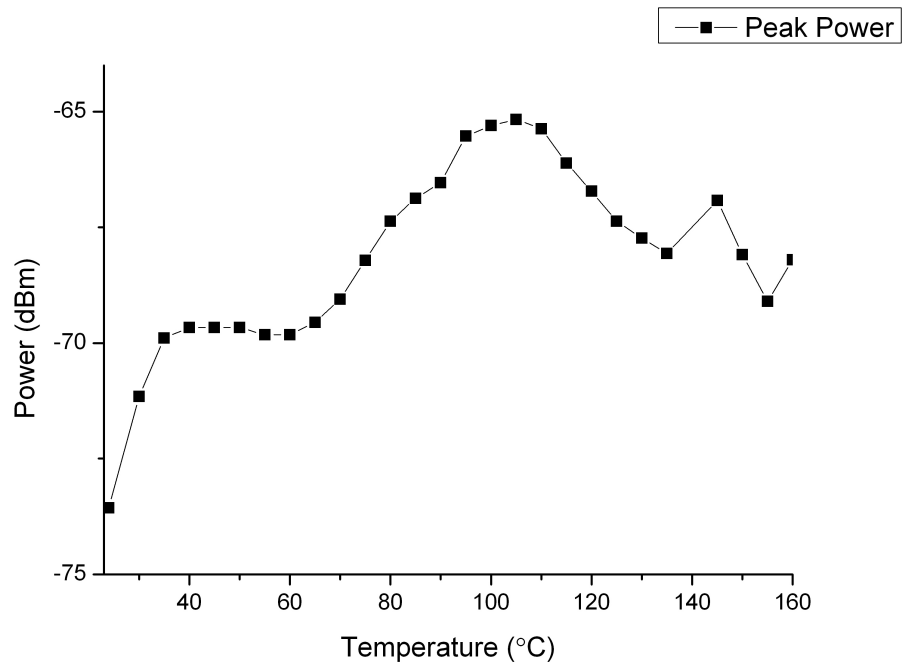


Figure 2.26

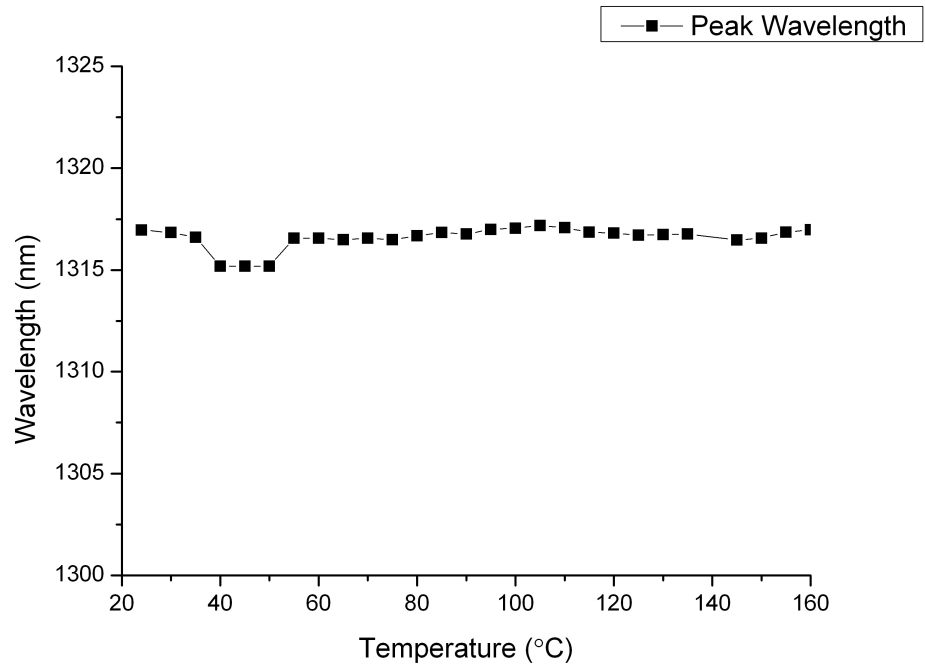


Figure 2.27

2.5 Single-mode Multi-mode Single-mode Sensor Fiber

Among different sorts of fiber sensors, Single mode-Multimode - Single mode (SMS) optical fiber sensors received extraordinary consideration over the most recent couple of years since they are easy to manufacture and low cost. In addition, being interferometric sensors, they are highly sensitive while they have high loss as well. A simple SMS sensor is composed of a short section of multimode (MM) fiber spliced between two single mode (SM) fibers.

Obviously in this experiment the middle fiber type is a multimode and the splicing state for the first sample is misaligned. We increase the temperature from room temperature to 150 °C and record the power spectrum changes which is illustrated in figure 2.28. In this experiment, as it is observable from figure 2.29 and figure 2.30, variation of a point on the power axis and wavelength axis for different temperature is not ascending or descending and we are in fact faced to some sudden changes. These sudden changes occur at 90 °C in this sample. The power amount for the selected point (power: -50.99dBm, temperature: 25.8 °C, wavelength: 1311.805nm) at the 90 °C falls to -55.36dBm and it rises again at 150 °C to -50.35dBm rapidly. It has an ascending trend along the wavelength axis up to 80 °C where it reaches 1319.84nm however the curve falls to 1304.1nm while the temperature increases 25 °C meaning at the temperature equal to 105°C, then the curve stays almost still up to 160 °C.

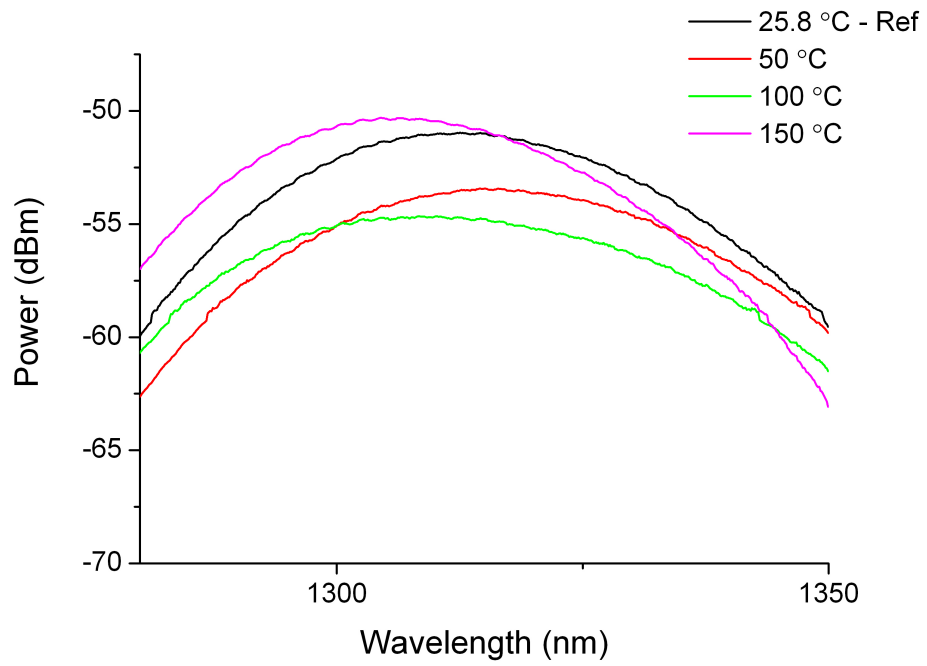


Figure 2.28

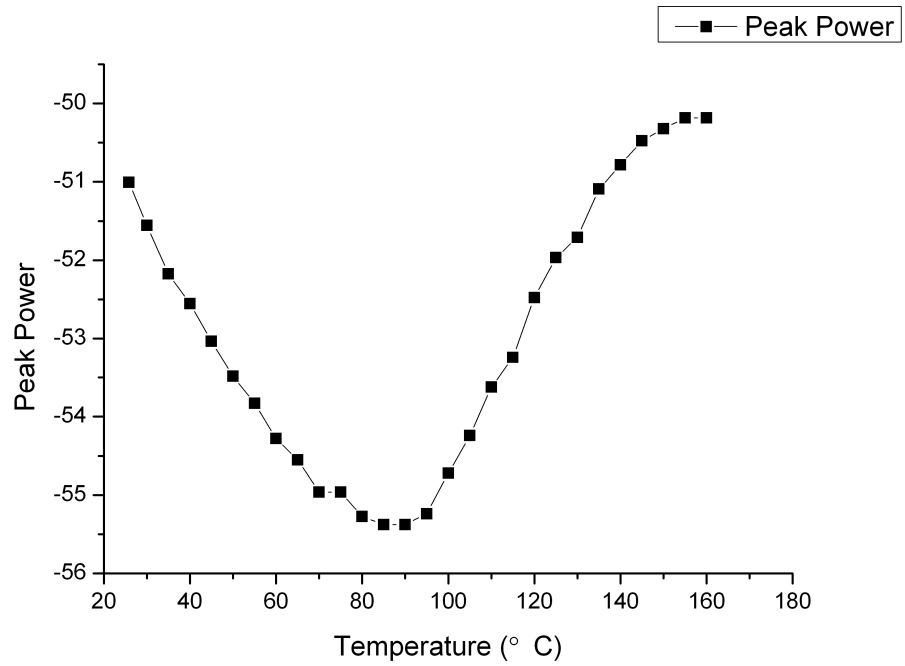


Figure 2.29

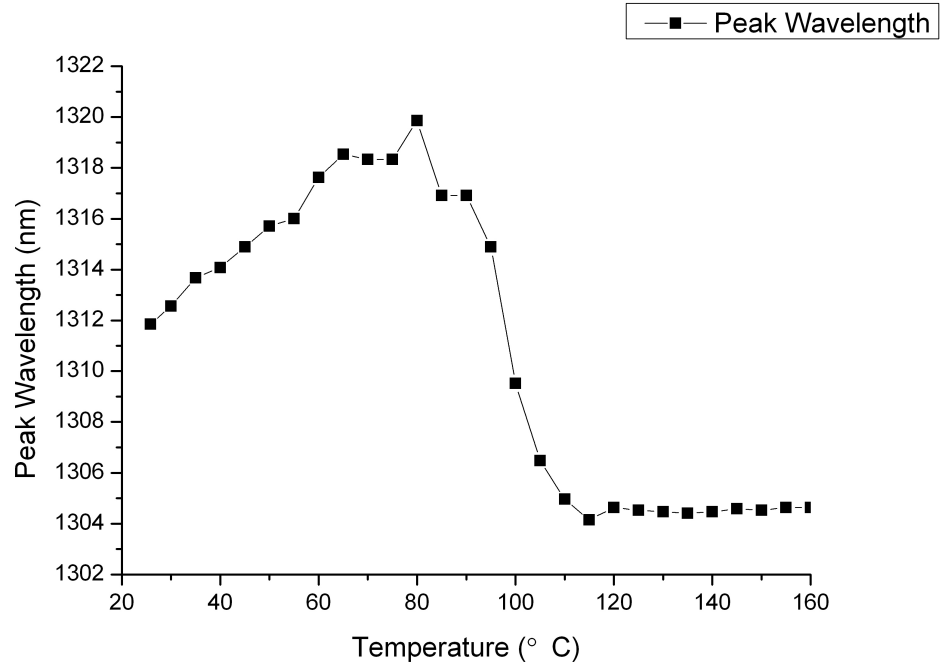


Figure 2.30

To have a regular variation in second sample, we considered the multimode part in the sensor with longer length. Similarly, in this sample the splicing state is $5\ \mu\text{m}$ misaligned for both ends of multimode fiber. Figure 2.31 shows the effect of temperature over power spectrum of the sensor. The peak power raises by increment in temperature. Figure 2.32 shows the curve ascending from -52.23dB to -47.095dB which is almost 5.135dB .

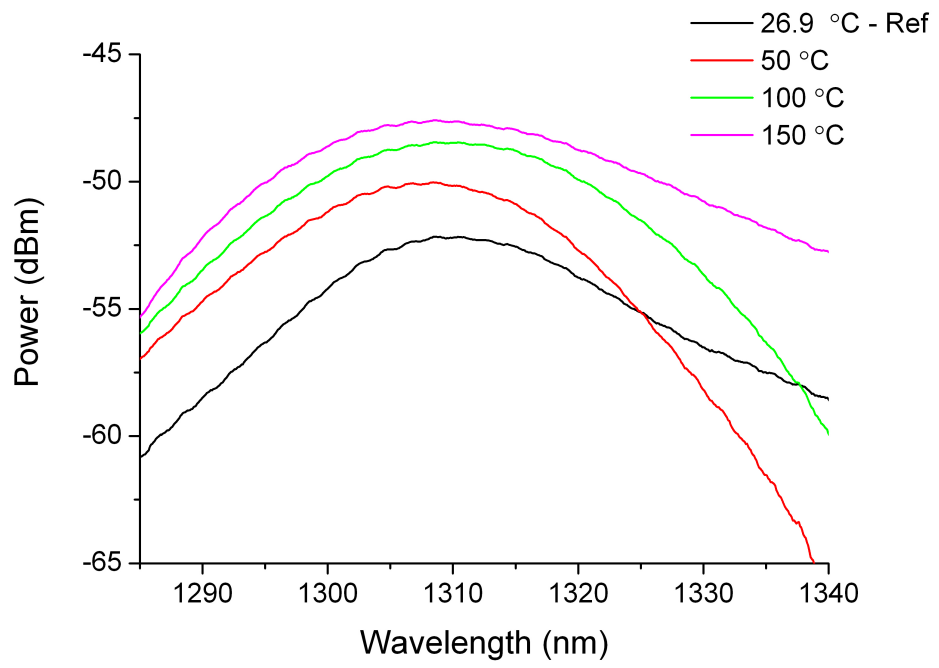


Figure 2.31

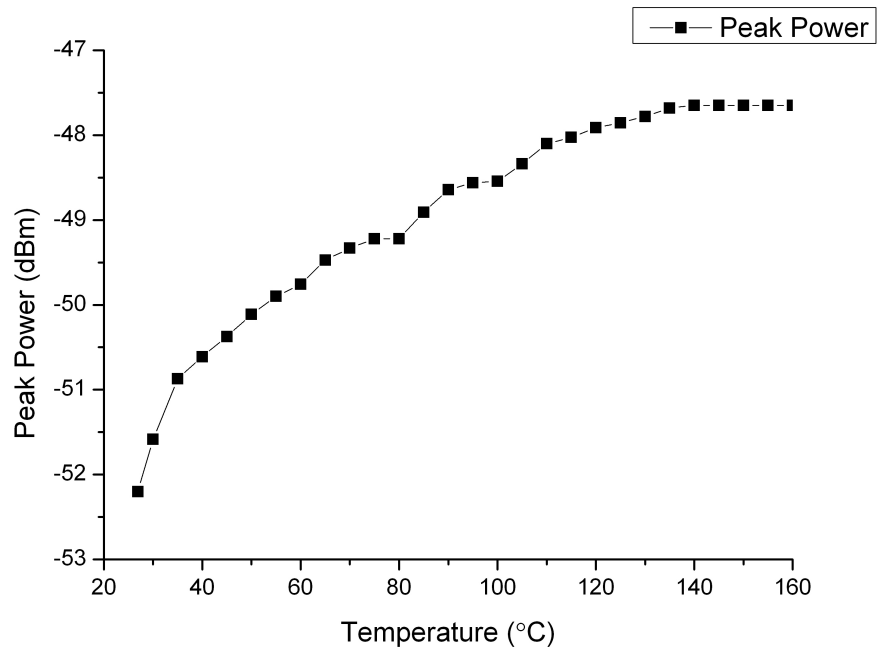


Figure 2.32

However, according to figure 2.33 variation is not noticeable along wavelength axis and the peak wavelength has a slight variation around 1309.41 nm.

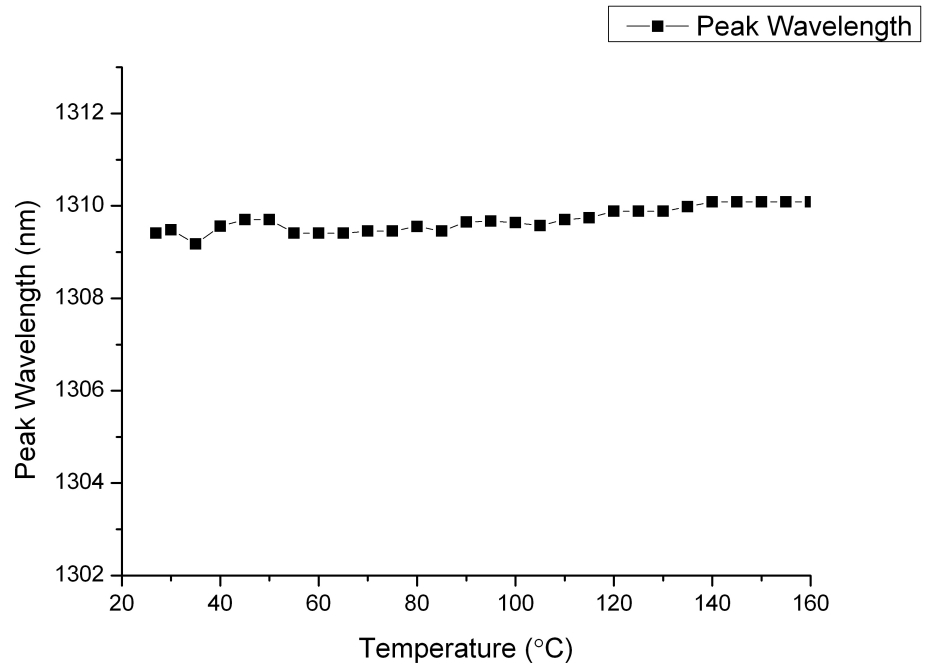


Figure 2.33

In the third sample, we examined the SMS sensor in the aligned state. As it is observed in figure 2.34 the power spectrum variation against temperature increment is inconsiderable. Both figure 2.35 and figure 2.36 verify this fact. In this sample by increasing the temperature, power variation for an arbitrary point from -42.5dBm moved only 0.5 dBm to reach -42dBm. In addition, the wavelength shifted 3nm from 1311 to 1308 which considered to be very small.

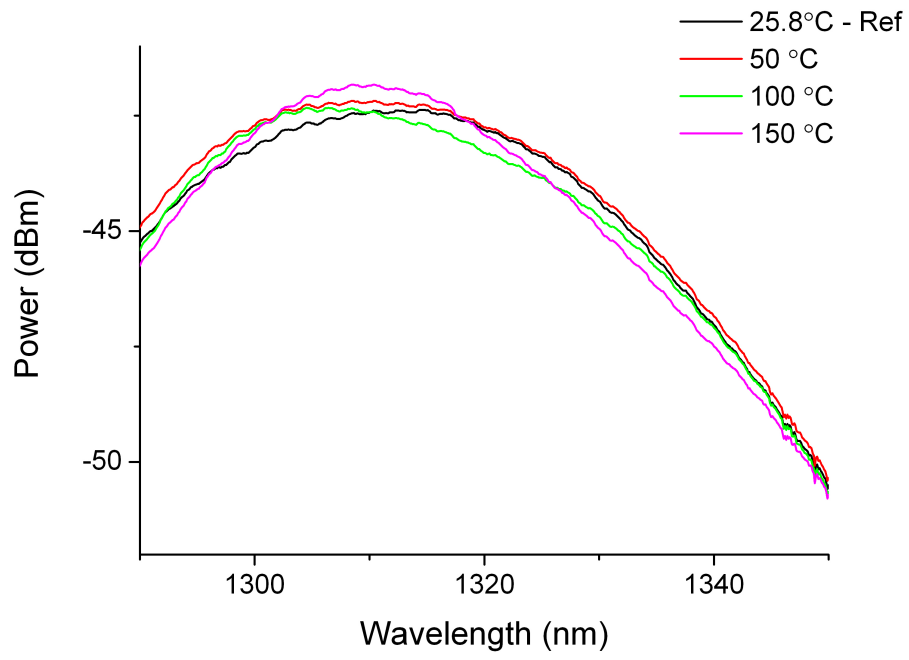


Figure 2.34

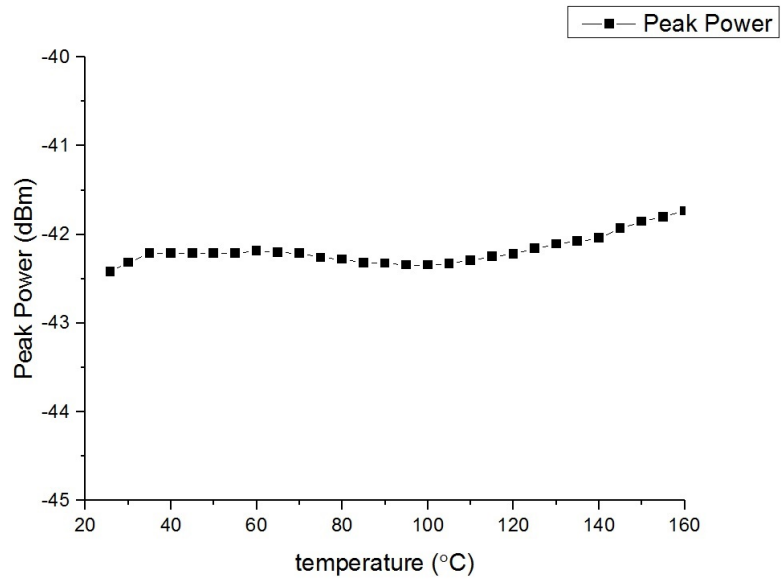


Figure 2.35

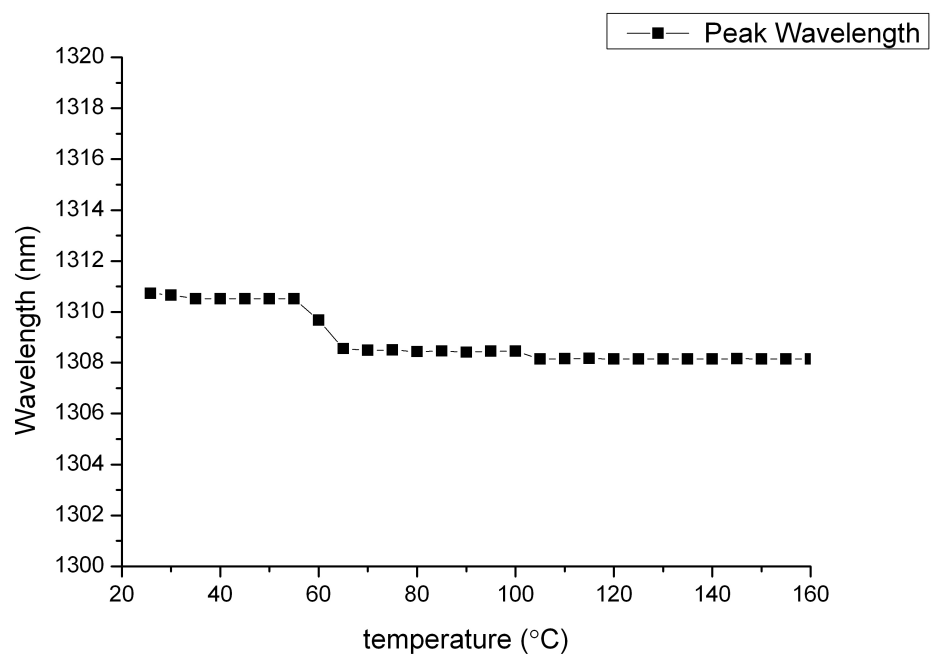


Figure 2.36

2.6 SM2000

For the last sample, we produced the sensor by splicing a piece of SM2000 fiber to two single mode fibers in misaligned state. Based on SM2000 characteristics, we measured the results in two different wavelength 1300nm and 1550nm. The cut of frequency in this fiber is around 1700nm. The temperature effect on this sensor is traceable in figure 2.37 and figure 2.38. The interesting note is the difference in wavelength shift of an arbitrary point (for instance an arbitrary peak point) in two different position one around 1300nm and one around 1550nm.

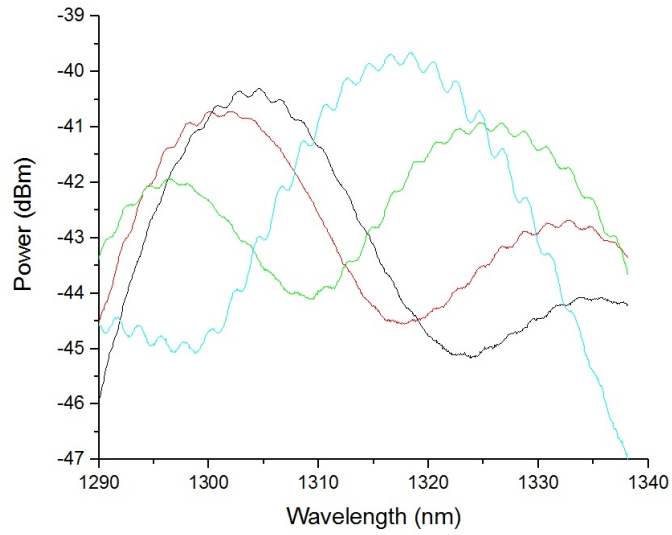


Figure 2.37

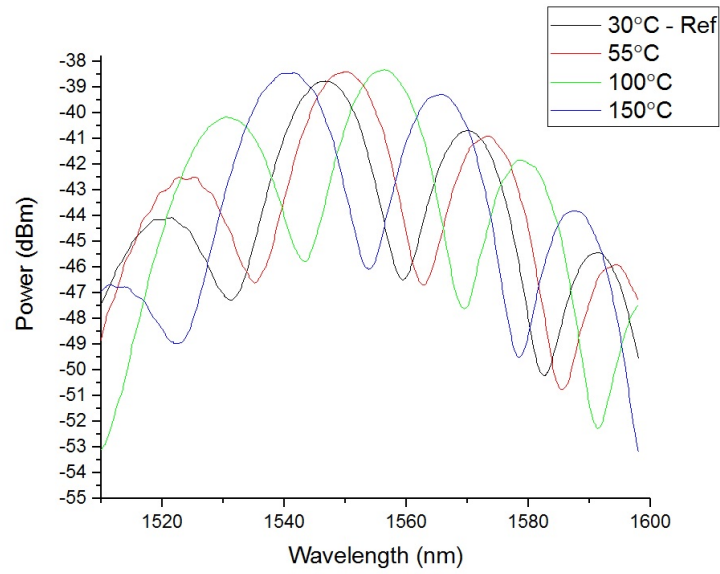


Figure 2.38

According to figure 2.39, the chosen point around 1300nm shifts backward by increasing the temperature which is quite opposite all other samples that we studied so far. The shift backward measurement is approximately 13.7nm (max:1304.451nm and min: 1290.75nm) by increasing the temperature from room temperature up to 160 °C.

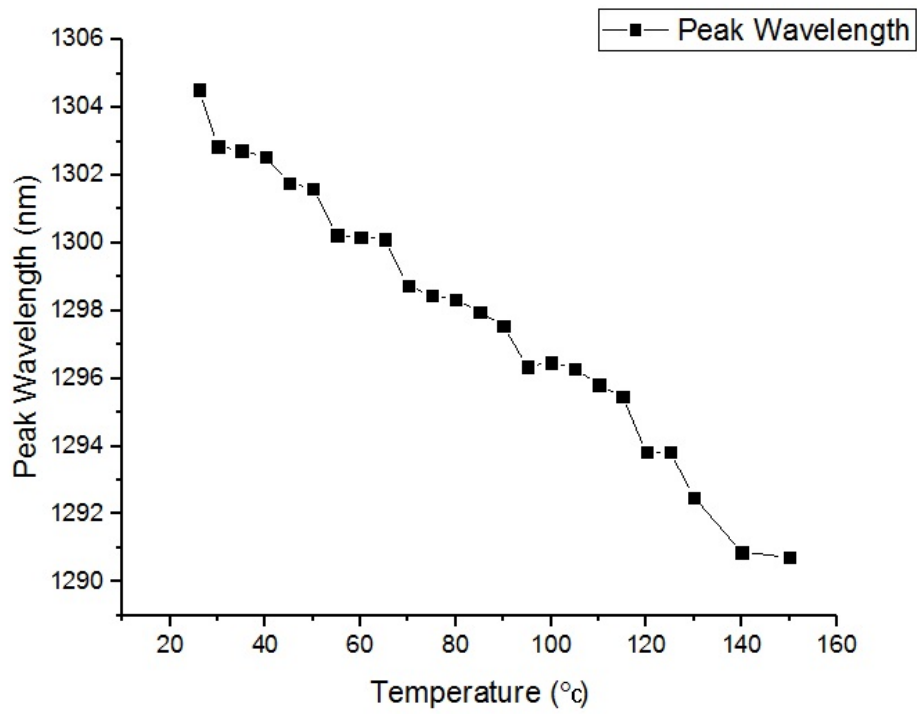


Figure 2.39

According to figure 2.40 by increasing the temperature, the selected point around 1550nm shifts forward. In this sample by increasing the temperature from room temperature up to 160 °C, there is 18.89nm shift (min: 1546.66nm and max: 1565.55nm) along wavelength axis.

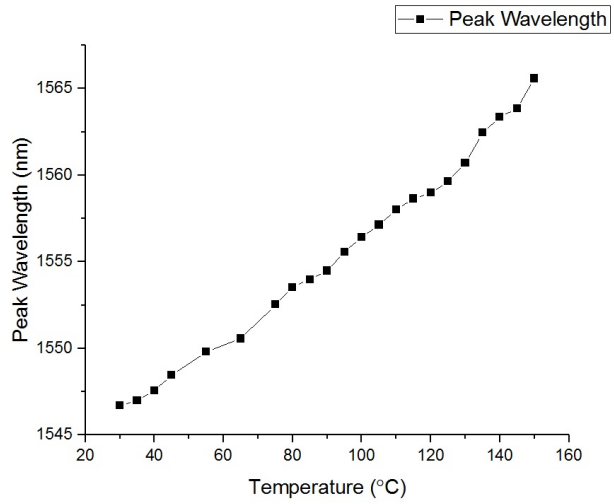


Figure 2.40

The power variation in two points of this sample is traceable in figure 2.41 and figure 2.42.

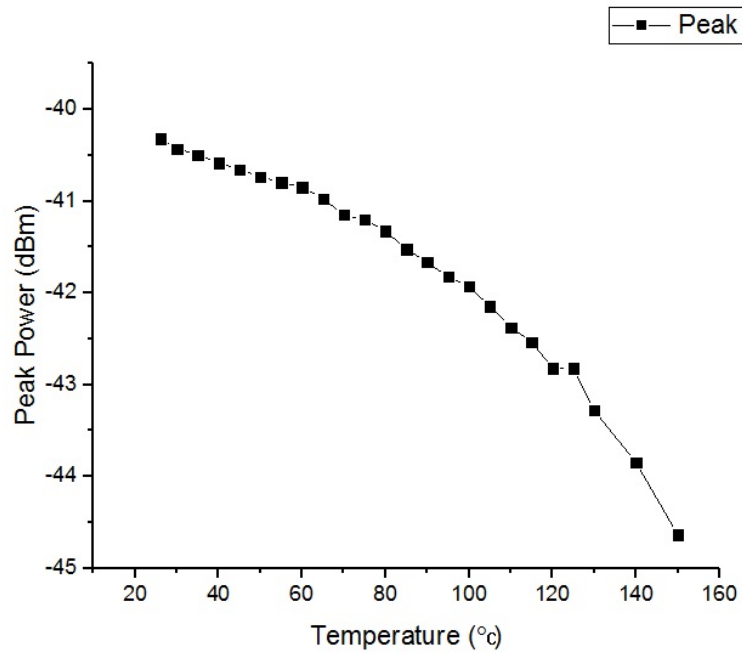


Figure 2.41

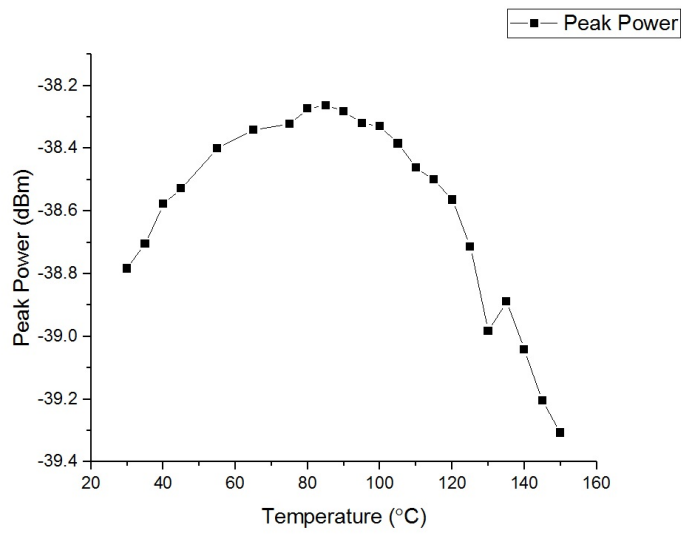


Figure 2.42

Chapter 3

Conclusion

In In this thesis, I studied the theory of waveform deformation in sensors and the effect of heat on the shape of the power spectrum plus changes in wavelengths and shifts in power levels in a practical experience. I constructed a variety of sensors which the multimode part includes BIF, Coreless fiber, SM2000 fiber, multimode fiber With 5 °C thermal intervals. My lab framework included an optical source, an OSA, a heater and a thermometer. The sensor fibre connected to the source from one end and to OSA from other end and it is placed over a heater. OSA connected to a PC too and captures the results. A separate thermometer precisely measures the heater temperature and send it to PC. The general experimental routine is to turn on the heater and every 5 °C interval record the power spectrum changes via OSA. The numerical data results analysed with a software called OriginLab.

The results of the practical section show that, as expected, the wavelength shift in a specific peak occurs only on SMS sensors that are made in misaligned. Of all types of SMS sensors, the SMS-SM2000 and SMS-BIF have a smooth wavelength diagram, and they are also significantly sensitive to heat rise. These two types of sensors, along with the SMS-Multimode, return to the original power spectrum diagram after cooling back to the room temperature, while this does not happen in the coreless, and the two power spectrum curves before the warming up and after cooling down are not matching. Another important point about the SMS-Multimode is that despite the significant shift in the wavelength with increasing heat, i.e. the high sensitivity to changes in temperature, their curves

are not smooth and the changes are not uniform.

The following table summarizes the results of wavelength shifts in a specified peak with increasing temperature.

| <i>SMS Type</i> | <i>Peak Wavelength Shift</i> | <i>Wavelength Curve</i> |
|-------------------------------|------------------------------|-------------------------|
| <i>BIF</i> | <i>16 nm</i> | <i>Smooth Curve</i> |
| <i>BIF</i> | <i>11.4872 nm</i> | <i>Smooth Curve</i> |
| <i>Coreless</i> | <i>0</i> | <i>---</i> |
| <i>Multi-mode</i> | <i>15.7</i> | <i>---</i> |
| <i>Multi-Mode (Long Case)</i> | <i>0</i> | <i>---</i> |
| <i>SM2000 (1300 nm)</i> | <i>13.7</i> | <i>Smooth Curve</i> |
| <i>SM2000 (1550 nm)</i> | <i>18.85</i> | <i>Smooth Curve</i> |

Figure 3.1: Comparison of the final results of misaligned configuration for different types

Chapter 4

Future Study

For further research in the future, two cases are considered: The first is to compare the behavior and stability of the similar SMS sensor fibers. For this purpose by reproducing a specific type of SMS sensor, we tried to produce similar sensors and compare them. The important point in this experiment was that the distance between two peaks was often the same. The figure 4.1 displays the board SM-Sensor SM2000 is built on it.

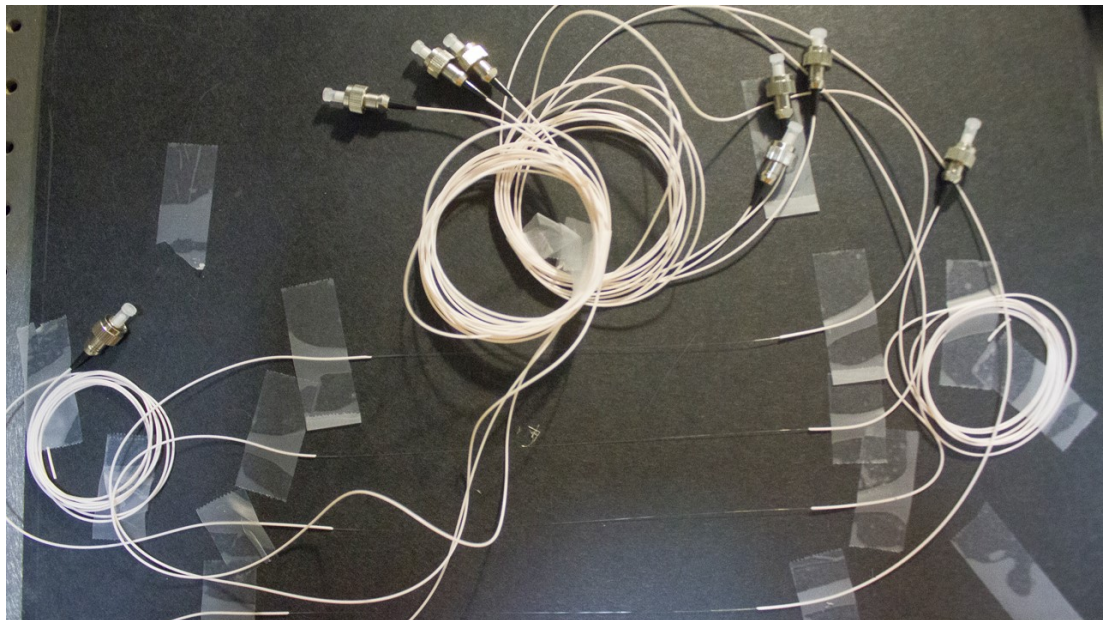


Figure 4.1

The second proposed case is the review of the behavior of two SMS sensor fibers, which are attached together in a cascade form, and to study the effect of heat on them. Fourier numerical analysis, especially with emphasis on peaks, is

suggested for this section. The figure 4.2 represent the framework, and the figure 4.3 shows the power spectrum at room temperature and the figure 4.4 comparing the power spectrum of the sensor at room temperature, 50 ° C and 100 ° C.

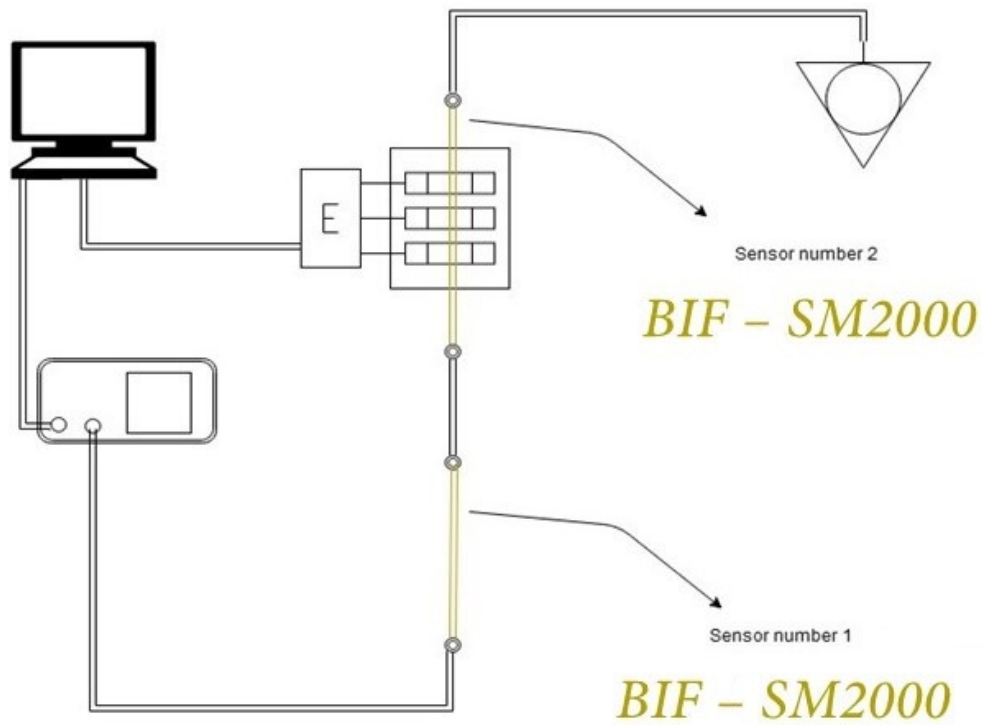
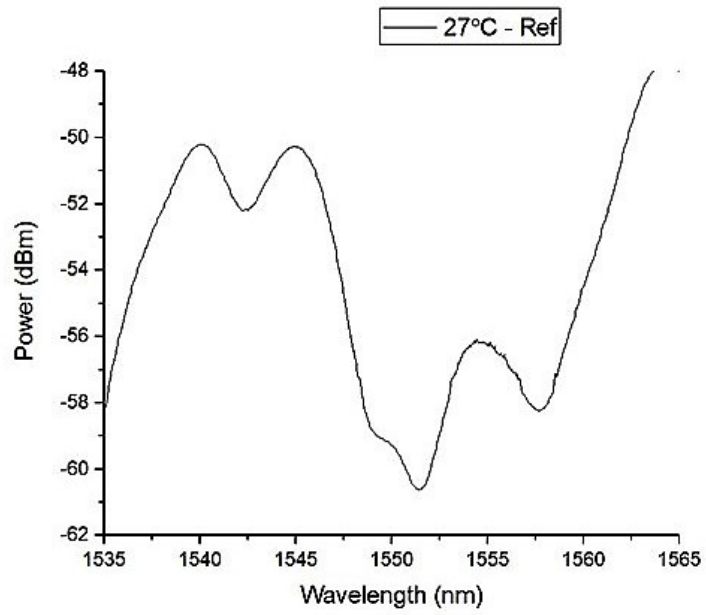
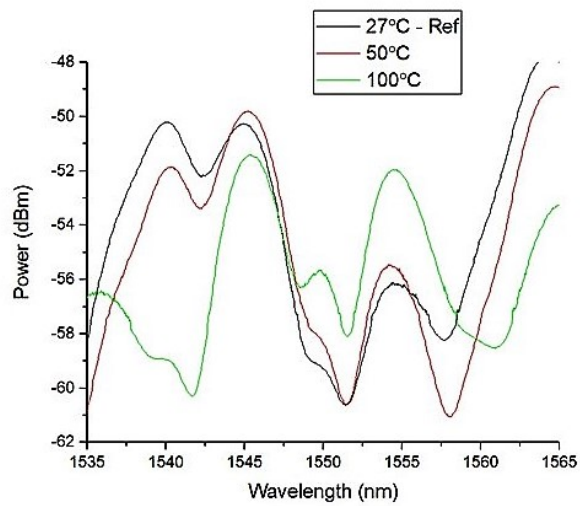


Figure 4.2



Misaligned Cascade SMS Sensor Fiber , BIF

Figure 4.3



Misaligned Cascade SMS Sensor Fiber , BIF

Figure 4.4

Bibliography

- [1] Q. Wang G. Rajan P. Wang A. M. Hatta, G. Farrell and Y. Semenova. Ratiometric wavelength monitor based on singlemode-multimodesinglemode fibre structure . *Microw. Opt. Technol. Lett.*, 50, 2008.
- [2] Q. Wu A. M. Hatta, Y. Semenova and G. Farrell. "Strain sensor based on a pair of single-mode-multimode-single-mode fiber structures in a ratiometric power measurement scheme" . *Appl. Opt.*, 49:536–541, 2010.
- [3] J. Bures. Guided Optics: Optical Fibres and All-fibre Components . *Wiley-CVH*, -, 2009.
- [4] X. Wen J. Li J. Zheng H. You H. Chen C. Zhang C. Li, T. Ning and W. Jian. Strain and temperature discrimination using a fiber Bragg grating and multimode interference effects . *Opt. Commun*, 343:6–9, 2015.
- [5] D. C. Chang and E. F. Kuester. A hybrid method for paraxial beam propagation in multimode optical waveguides . *Trans. Microwave Theory Tech*, 29, 1981.
- [6] W.-K. Liu Y. Liu D.-P. Zhou, L. Wei and J. W. Y. Li. "Simultaneous measurement for strain and temperature using fiber Bragg gratings and multimode fibers" . *Appl. Opt.*, 47:1668–1672, 2008.
- [7] G. Farrell Q. Wang G. Rajan, Y. Semenova and P. Wang. A low polarization sensitivity all-fibre wavelength measurement system . *Photon. Technol. Lett*, 20, 2008.
- [8] P. Wang G. Rajan, Y. Semenova and G. Farrell. Temperature-induced

- instabilities in macro-bend fibre-based wavelength measurement systems .
J. Lightw. Technol, 27, 2009.
- [9] Y. Semenova G. Farrell G. Rajan, Q. Wang and P. Wang. Effect of polarization dependent loss on the performance accuracy of a ratiometric wavelength measurement system . *IET Optoelectronics*, 2, 2008.
- [10] L. Li A. Schlzgen N. Peyghambarian H. Li, M. Brio and J. V.Moloney. Multimode interference in circular step-index fibres studied with the mode expansion approach . *J. Opt. Soc. Am. B, Opt. Phys*, 24, 2007.
- [11] X. Zhang L. Yuan Z. Yang H. Sun, S. Yang and M. Hu. "Simultaneous measurement of temperature and strain or temperature and curvature based on an optical fiber MachZehnder interferometer" . *Opt. Commun*, 340:39–43, 2015.
- [12] J.Sanchez-Mondragon J. E. Antonio-Lopez, P. LiKamWa and D.A. May-Arrijoa. "All-fiber multimode interference micro-displacement sensor" . *Meas. Sci. Technol*, 24:55104–55107, 2013.
- [13] S. Wang B. Li M. Wang H. Xiao Y. Lu J. Yang, L. Jiang and H. Tsai. High sensitivity of taper-based MachZehnder interferometer embedded in a thinned optical fiber for refractive index sensing . *Appl.Opt.*, 50:5503–5507, 2011.
- [14] E. Li. Temperature compensation of multimode-interference-based fibre devices . *Opt. Lett*, 32, 2007.
- [15] G. Perrone A. Vallan L. Greborio P. Regio M. Olivero, R. Orta and P.Pellegrino. Multipath interference characterization of bend-insensitive fibers for short-reach optical communications . *Proc. SPIE*, 9525:1–7, 2015.
- [16] R. Orta M. Olivero and G. Perrone. Equivalent radial transmission lines for the computation of guided modes in trench-assisted bendinsensitive fibers .
submitted to J. Opt. Soc. Am. B., -.

- [17] R. Orta P. Pellegrino G. Perrone M. Olivero, L. Greborio and P. Regio. Multipath interference characterization of bend-insensitive optical fibers and short jumpers . *Appl. Opt.*, 55:2998–3005, 2016.
- [18] Renato Orta Guido Perrone Massimo Olivero, Alberto Vallan. "Single mode-multimode-single mode optical fiber sensors: review and application to temperature measurements using a bend-insensitive fiber" . *IEEE Xplore*, 7 July 2017.
- [19] K. Sooley P. Lu, L. Men and Q. Chen. "Tapered fiber MachZehnder interferometer for simultaneous measurement of refractive index and temperature" . *Appl. Phys. Lett.*, 94:pp. 1311102pp, 2009.
- [20] G. Farrell Q. Wang and T. Freir. Study of transmission response of edge filters employed in wavelength measurements . *App. Opt*, 44, 2005.
- [21] G. Farrell Q. Wang and W. Yan. "Investigation on single - mode multimode single - mode fiber structure" . *J. Light. Technol.*, 26:512–519, 2008.
- [22] G. Farrell Q. Wang and W. Yan. Investigation on singlemode-multimodesinglemode fibre structure . *J. Lightw. Technol*, 26, 2008.
- [23] G. Farrell Q. Wang and W. Yan. Investigation on singlemodemultimode-singlemode fibre structure . *J. Lightw. Technol*, 26, 2008.
- [24] P. Wang Q. Wang, G. Rajan and G. Farrell. Resolution investigation of a ratiometric wavelength measurement system . *App. Opt*, 46, 2007.
- [25] T. Freir G. Rajan Q. Wang, G. Farrell and P. Wang. Low-cost wavelength measurement based on a macrobending single-mode fibre . *Opt.Lett*, 31, 2006.
- [26] B. Yan Y. Ma P. Wang C. Yu Q. Wu, Y. Semenova and G. Farrell. "Fiber refractometer based on a fiber Bragg grating and single modemulti modesingle mode fiber structure" . *Opt. Lett*, 36:2197–2199, 2011.
- [27] A. Vallan M. Konstantaki S. Pissadakis R. Gassino, Y. Liu and G. Perrone. A fiber optic probe for tumor laser ablation with integrated temperature measurement capability . *accepted J. Lightwave Technol*, 2016.

- [28] G. Rajan. A macro-bend fibre-based wavelength demodulation system for optical fibre sensing applications . *Dublin Institute of Technology*, -, 2008.
- [29] K. Liu S. M. Melle and R. M. Measures. Practical fibre-optic Bragg grating strain gauge system . *App. Opt*, 32, 1993.
- [30] R. K. Varshney Y. B. P. Kumar E. Marin S. M. Tripathi, A. Kumar and J.P. Meunier. Strain and temperature sensing characteristics of single-mode multimode single-mode structures . *J. Lightw. Technol*, 27, 2009.
- [31] M. A. R. Franco J. G. Hayashi F. X. Malcata O. Frazao P. Jorge S. Silva, E. G. P. Pachon and C. M. B. Cordeiro. "Ultra-high-sensitivity temperature fiber sensor based on multimode interference" . *Appl. Opt*, 51(2):3236–3242, 2012.
- [32] L.B. Soldano and E.C.M. Pennings. Optical multi-mode interference devices based on self-imaging: principles and applications . *J. Lighthw. Techno*, 13, 1995.
- [33] L.B. Soldano and E.C.M. Pennings. Optical multi-mode interference devices based on self-imaging: principles and applications . *J. Lighthw. Technol*, 13, 1995.
- [34] M. H. Abu Bakar Y. M. Kamil T. K. Yadav, R. Narayanaswamy and M. A. Mahdi. Single mode tapered fiber-optic interferometer based refractive index sensor and its application to protein sensing . *Opt.Express*, 22:22802–22807, 2014.
- [35] Zhaobing Tian and S. S.-H. Yam. In-Line Abrupt Taper Optical Fiber MachZehnder Interferometric Strain Sensor . *IEEE Photonics Technol.Lett.*, 21:161–163, 2009.
- [36] International Telecommunication Union. ITU-T G.650.1- Definitions and test methods for linear, deterministic attributes of single-mode fibre and cable . -, 2012.

- [37] P. W. E. Smith W. S. Mohammed and X. Gu. All-fibre multimode-interference-based refractometer sensor: proposal and design . *Opt. Lett*, 31, 2006.
- [38] X. Gu W. S. Mohammed, P. W. E. Smith. All-fibre multimode interference bandpass filter . *Opt. Lett*, 31, 2006.
- [39] Q. Wang and G. Farrell. All-fibre multimode-interference-based refractometer sensor: proposal and design . *Opt. Lett*, 31, 2006.
- [40] Q. Wang and G. Farrell. All-fibre multimode-interference-based refractometer sensor: proposal and design . *Opt. Lett*, 31, 2006.
- [41] Q. Wang and G. Farrell. Multimode-fibre-based edge filter for optical wavelength measurement application and its design, . *Microw. Opt. Technol. Lett.*, 48, 2006.
- [42] A. Yablon. Optical Fiber Fusion Splicing . *Berlin/Heidelberg: Springer-Verlag*, 103, 2005.
- [43] A. Yablon. Optical Fiber Fusion Splicing . *Berlin/Heidelberg: Springer-Verlag*, 103, 2005.
- [44] J. Yamauchi. Propagating Beam Analysis of Optical Waveguides . *Research Studies Press*, -, 2003.